Received: 1 March 2022 | Revised: 28 March 2022 | Accepted: 28 March 2022

DOI: 10.1002/pol.20220122

REVIEW

JOURNAL OF POLYMER SCIENCE WILEY

Mesoporous carbons from self-assembled polymers

Mark Robertson | **Moustafa M. Zagho** | **Sergei Nazarenko** | **Zhe Qiang**

School of Polymer Science and Engineering, University of Southern Mississippi, Hattiesburg, Mississippi, USA

Correspondence
Zhe Qiang, School of Polymer Science and Engineering, University of Southern Mississippi, Hattiesburg, MS 39406, USA.
Email: zhe.qiang@usm.edu

Funding information
National Science Foundation, Grant/Award Numbers: OIA-1757220, DGE-1449999

Abstract

Polymer self-assembly provides a robust and cost-efficient nanomanufacturing platform for enabling a broad range of applications, such as microelectronics, drug delivery, and separation membranes. This review focuses on discussing the progress and opportunities of self-assembled polymer in the synthesis of mesoporous carbons (MCs), which have aroused significant research interests over the past decades. Specifically, we will discuss the two most established approaches for converting nanostructured polymers to MCs, including templating-based and direct pyrolysis-based methods. We will also review the fundamental ordering mechanisms and kinetics of these polymeric systems and discuss the recent development of engineering methods for providing on-demand control over the pore size and morphology of MCs. Additionally, this review article also includes a section focusing on the strategies to further functionalize these materials from self-assembled polymers to enhance their performance, such as chemical activation, heteroatom doping, introduction of nanoparticles into the carbon matrix, and enhancing graphitization degree of carbon walls. Finally, a brief perspective is provided about the emerging research opportunity in this exciting field.

KEYWORDS

nanostructures, porous carbons, pyrolysis, self-assembly, template

1 | INTRODUCTION

Porous carbon materials are used in many applications due to their inherent thermal and electrical conductivity, chemical inertness, and the ability to interact with specific molecules as they diffuse into the carbon matrix.[1,2] These materials are often defined in terms of pore sizes where microporous, mesoporous, and macroporous carbons correspond to pores below 2 nm, between 2 and 50 nm, and greater than 50 nm, respectively. Generally, microporous carbons are advantageous in terms of their high surface area due to the large amount of micropores but suffer from limited mass transport capabilities due to the restricted pore sizes.[3–5] Macroporous carbons provide greatly enhanced mass transport into the carbon matrix, but the large pore sizes result in very low surface areas ($<50\ m^2/g$), limiting the amount of sorption sites for guest molecules to interact with the carbon matrix.[6,7] For many applications, mesoporous carbons provide a marriage of the advantages of microporous and macroporous systems where the pore sizes are sufficiently large to facilitate mass transport of guest molecules while retaining relatively high surface area ($>200\ m^2/g$). The pore sizes are also important in providing size-selective adsorption of molecules, which can become increasingly important in environmental remediation applications. Furthermore, establishing long-range order of interconnected pore channels within these systems provides less tortuous pathways for guest molecules to diffuse into the carbon matrix compared to disordered carbons. Therefore, mesoporous carbons (MCs) have received significant research interests over the past decades due to their distinct

advantages compared to activated carbon, which is the most common porous carbon and indispensable in various modern applications,[8–11] including synthetic flexibility in tuning the pore size and matrix chemistry, uniform pore structures with excellent accessibility, and enhanced mass transport within the pore channels.[12–14] Combining these unique properties enables MC to become a very promising material candidate in diverse fields such as separation membranes,[15–17] sensors,[18,19] electrodes for batteries,[20–23] catalyst support,[24–26] supercapacitors,[27–29] and adsorbents for water purification.[30–33] To date, the most successful strategies for synthesizing MCs include templating-based methods (both soft-templating and hard-templating) and directly pyrolyzing microphase-separated carbon precursors.[34–38] For both approaches, self-assembly of polymers is a key enabler to produce ordered, nano-size features prior to crosslinking and carbonization steps. As a canonical system, surfactants and/or block copolymers (BCP) can spontaneously generate periodic nanostructures due to the incompatibility between their covalently linked, chemically distinct segments, while providing precise control over the resulting pattern size and morphology through manipulating the chemical composition and physical properties.[39–42] In MC systems, these nanostructures consist of sacrificial segments in the minority phase which can be thermally decomposed to produce pores, and carbon precursors in the majority phase which produces high degrees of carbon yield upon exposure to temperatures above 600 °C in inert atmospheres. For example, the conversion of resol and polyacrylonitrile to carbon upon pyrolysis have been investigated by many studies.[43,44] Generally, these templates are thermodynamically driven to self-assemble into ordered nanostructures due to chemical dissimilarities between the covalently bound segments of the surfactant/BCP. In these systems, phase separation occurs as the product of the Flory-Huggins interaction parameter between the segments and the degree of polymerization (χN, or segregation strength) increases beyond 10.5. The overall hydrophilic volume fraction, contributing from both template and carbon precursor (which is often hydrophilic), dictates the morphologies and feature sizes of the self-assembled domains, which is very similar to the classical BCP self-assembly.[45] The assembly process is often a product of competition between both thermodynamic and kinetic factors, where non-equilibrium morphologies can be kinetically trapped as discussed in Section 4. Since the inception of MC, its development has largely relied on the use of self-assembled polymers. Notably, even for hard-templating methods, which utilize mesoporous inorganics (e.g., silica) to direct the nanostructures of carbon precursors, their processes also involve the self-assembly of surfactants/block copolymers (BCPs) for preparing the hard template.[46–49] However, considering there are already many outstanding reviews on the topic of MC synthesis and applications, this hard-templating method will not be covered in this article.[12,14,50]

This review primarily focuses on self-assembled polymers for MC synthesis, particularly regarding the recent advances in material selection, engineering methods, and system design for controlling the morphology, pore textures, and functionality of their derived porous carbons. Specifically, we will discuss both soft-templating and direct pyrolysis methods in the following two sections. For the first system, it is important to understand the fundamental ordering mechanism and kinetics of surfactants and/or BCPs during the annealing step with the presence of carbon precursors. Moreover, we will discuss the evolution of mesostructures within these polymeric templates/precursors in each processing stage, from the as-cast to carbonized state, as well as review efficient annealing methods for producing long-range ordering and/or directional pore channels. Obtaining on-demand control over the degree of ordering and pore size in MCs is critical for attaining the desired material properties. Additionally, research efforts to tailor or further functionalize MCs will be covered, including increasing surface area, chemical modification of carbon framework, and introduction of nanoparticles for enhancing their performance. Finally, we provide a very brief viewpoint on the main challenges that need to be addressed for enabling the broader use of MCs in practical applications.

2 | TEMPLATING-BASED METHODS

Self-assembly of amphiphilic surfactants and block copolymers (BCPs) enables facile preparation of ordered functional nanomaterials with direct access to a wide variety of different structures and domain sizes.[51–53] Leveraging this advantage, Kresge et al. reported one of the very first examples of using a surfactant-mediated self-assembly approach to fabricate a family of mesoporous silicas, of which the pore sizes can be tailored upon the selection of surfactant type, reaction condition, and auxiliary chemicals.[54] This work pioneered the synthesis of mesoporous solids from calcination of inorganic gels with the presence of surfactants, establishing an important synthetic platform which employs an amphiphilic organic component as the nanostructure templating agent for directing the assembly of inorganic precursors. This soft-templating method was then broadly applied for synthesizing MCs with phenolic resin (resol) being the most

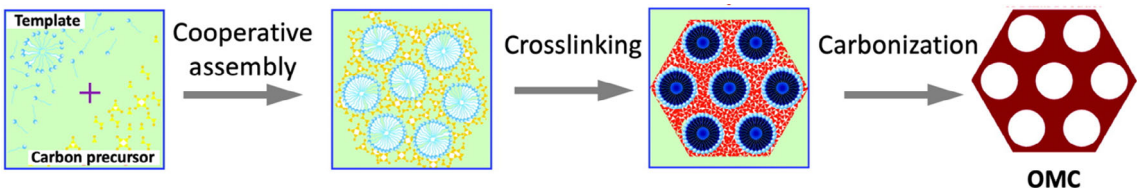

FIGURE 1 Synthesis of MCs through an established soft-templating method.[56] The cooperative assembly of template molecules and carbon precursors enables the formation of ordered nanostructures. Upon subsequent crosslinking and carbonization steps, the precursors can be converted to carbon matrix, while the polymer template is thermally decomposed to create pores. Reprinted with permission from Wan and Zhao.[56] Copyright 2007. American Chemical Society

common carbon precursors. Following briefly describes the critical considerations in the system design for preparing MCs using soft-templating method: i) carbon precursors need to have favorable interactions with selective components of the templates for cooperative assembly without the occurrence of macrophase separation, ii) templating agents can be fully decomposed upon calcination/carbonization for efficiently creating mesopores within the inorganic frameworks, and iii) carbon precursors should provide sufficient mechanical integrity for retaining the nanostructures upon the removal of templates,[55] which is often achieved by forming crosslinked networks using thermoset materials. Figure 1 briefly illustrates the process of fabricating MCs using soft-templating method, involving steps of self-assembly, crosslinking, and carbonization.[56] This section summarizes the use of different types of nanostructured polymers as the templates for MC synthesis, including self-assembled amphiphilic surfactants and linear BCPs. Additionally, we will also discuss the recent advances in emerging polymer templates for their application in MC synthesis, which contain complex chain topology, such as bottlebrush and star-like architectures.

2.1 | Amphiphilic surfactant templates

Surfactant molecules are typically amphiphilic, such as containing a polar head group and a long hydrocarbon tail, which the head group can be either ionic or nonionic. When exposed to water, these molecules can aggregate into different nanostructures, including spheres, worm-like cylinders, and vesicles, with hydrophobic cores and hydrophilic shells.[57,58] In general, the morphology of surfactant aggregates depends on the overall volume fraction of hydrophilic components in the system.[59,60] There are extensive studies focusing on understanding the critical micelle concentration (CMC) of surfactant molecules,[61,62] an important concentration condition above which micelle formation becomes significant. Altering the CMC value provides additional handles for manipulating the nanostructures of amphiphilic surfactants. Typically, CMC can be influenced by the presence of additives (e.g., salts),[63–65] organic solvents (e.g., ethanol, methanol, and acetone),[66] as well as the solution temperature.[65,67] As this review primarily focuses on the synthesis of MCs from nanostructured polymers, readers who are interested in surfactant self-assembly are recommended to several other excellent reviews that are dedicated on the relevant topics.[57,58,68]

Early work of surfactant-templated MCs relied on the use of cetyltrimethylammonium bromide (CTAB) as the template and phenolic resin (resol) as the carbon precursor; these two components can be co-assembled into ordered mesophases through favorable Coulombic interactions.[69,70] Through altering their mass ratio, the overall volume fraction of hydrophilic component in the system can be effectively manipulated to attain different nanostructures, including spheres, cylinders, lamellae, and disordered phases. Additionally, domain spacing of these MCs can be controlled by varying the alkyl chain length of the surfactant, which typically has the range of 2.9–3.7 nm, or by changing the concentration of CTAB in the surfactant/precursor solutions during the synthesis.[71] More recently, cooperative assembly of CTAB and carbon precursor (aqueous mesophase pitch [AMP]) was extended to a system containing graphene oxide (GO) for producing mesoporous carbon microspheres/graphene composites. The assembly between multiple components was encouraged by the strong electrostatic interactions between CTAB and AMP.[72] In this work, it was found that both CTAB loading and solution aging temperature can dominantly determine the final structures and pore dimensions of these mesoporous carbon composites. Particularly, carbon microspheres containing pores with diameters of 30–40 nm can be formed and homogeneously distributed on the GO surfaces when the loading content of CTAB was in the range of 10.6–12.7 g/L and aging temperature was 140 °C. The optimized material composition, processing condition, and morphology led to the excellent performance of this MC/reduced GO composite for supercapacitor application, achieving

capacitance of 279 F/g at the current density of 1 A/g, which can be retained over 92% after 6000 cycles. Similar to the studies using micellar CTAB as the template, MC with interesting vesicular structure have also been demonstrated through the use of pitch (carbon precursor) and hexadecyltrimethylammonium bromide (HTAB, surfactant template).[70] By altering the pH value of aqueous solution (the assembly media), HTAB can be aggregated into worm-like structures. Subsequently, upon carbonization the resulting materials contained 2–4 nm pores and 5–30 nm wall thickness, of which the pores are all perpendicular to the walls of the carbon vesicles.

In addition to CTAB,[70] many other alkyl chain-based surfactants have been investigated as templating agents for preparing mesoporous carbons. For example, Meng et al., employed non-ionic Brij surfactants as the templating agent, while using resol as the carbon source.[45] In this work, despite the formation of highly ordered nanostructures through the multi-component self-assembly, the product after carbonization at 800 °C did not exhibit any porous structure, which was likely associated with the high carbon yield of templating surfactants that contain relatively long alkyl chains (i.e., Brij). This study confirms that complete decomposition of the template is necessary for the synthesis of MCs, which the pyrolyzed templates should be gaseous products. Furthermore, an inherent limitation of using these alkyl based-surfactants as structure-directing templates for synthesizing MCs is that they can only yield very small mesopores, typically no larger than 5 nm. This is because these surfactants are usually very low molecular weight molecules (<1500 g/mol), and thus their derived nanostructures inevitably have small feature sizes. To address this challenge, more studies have been focused on using BCPs as the templates for preparing mesoporous carbons.

2.2 | Linear block copolymer templates

BCPs typically consist of at least two or more chemically dissimilar homopolymers with covalent linkages. The immiscibility between different segments can drive the occurrence of a spontaneous nanoscale phase separation process provided that sufficient segregation forces are present within the system.[39,73] A distinct difference between surfactant (described in Section 2.1) and BCP assembly is that BCP can form ordered nanostructures in melt with the absence of solvent, while surfactant in bulk is often disordered due to either their low molecular weight or crystalline nature. As a result, the soft-templating method of synthesizing MCs from BCP templates often involves the mechanism of evaporation-induced self-assembly (EISA),[74] as the ordering of template/carbon precursor blends is primarily driven by the solvent drying process (their solution state may be disordered and homogeneous).[75–78] For comparison, surfactant-templating method can lead to ordered nanostructures in aqueous solution, which the solvent drying simply solidifies the as-formed nanostructures. Furthermore, a significantly broader range of morphologies is attainable from BCP self-assembly compared to their counterparts from surfactants, including A15 phases,[79–81] σ phases,[82] and many other quasicrystal phases.[83–85]

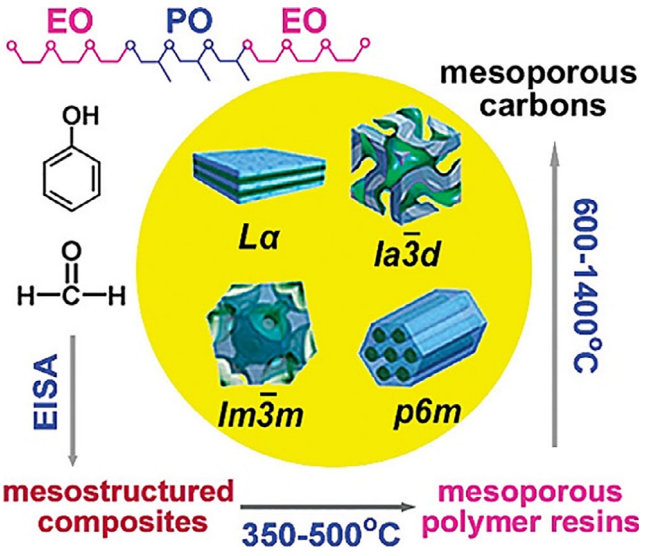

FIGURE 2 Synthesis of MC using linear block copolymer, PEO-*b*-PPO-*b*-PEO, as the template and resol as the carbon precursor.[45] Reprinted with permission from Meng et al.[45] Copyright 2006. American Chemical Society

One of the most widely used BCP templates in MC synthesis is the Pluronic family, which typically composed of linear poly(ethylene oxide)-*block*-poly(propylene oxide)-*block*-poly(ethylene oxide) (PEO-*b*-PPO-*b*-PEO) with different molecular weight and chemical composition. While in some literature they are recognized as the surfactant molecules, herein we categorize them as the linear BCPs due to two reasons: first, their assembly with carbon precursors involves the EISA mechanism for directing the nanostructure formation; second, they are composed of homopolymers with covalent linkages and their molecular weight is typically in the range of 2500–6000 g/mol, which is much higher than the alkyl-based surfactants (e.g., CTAB) discussed in the previous section.

In 2006, Meng et al., performed a comprehensive and systematic study on understanding how the template/precursor composition and processing condition impact the morphology, pore structures, and properties of their

derived MCs, using resol as the carbon precursor and three different Pluronic BCP (F127, P123, and F108) as the template. Figure 2 summarizes the key steps for the synthesis of MCs using Pluronic/resol system[45]: including 1) resol preparation, 2) formation of the mesostructures through EISA, 3) resol crosslinking by heating, 4) removal of the template by calcination at or above 350 °C, and finally 5) carbonization at 600 °C or higher, which converts the crosslinked polymer matrix to an amorphous carbon framework. It is important to note that resol can efficiently mix and strongly interact with the PEO segments within the Pluronic templates through hydrogen bonding, further driving the self-assembly process to occur while preventing the macrophase separation. Additionally, since Pluronic polymers typically have a relatively low thermal decomposition temperature (~300 °C),[86] mesoporous polymers can be developed upon calcination at 350 °C, confirmed by Fourier transform infrared (FTIR) spectrum, solid-state ^{13}C nuclear magnetic resonance (NMR) spectrum, and their nitrogen sorption isotherms. By varying the mass ratio between Pluronic template and resol, MCs containing a variety of different nanostructures, such as spheres with body centered cubic packing, 3D bicontinuous gyroids, and 2D hexagonally packed cylinders, can all be successfully obtained. It was found that by increasing the pyrolysis temperature from 400 to 800 °C, their pore size typically becomes smaller while the surface area of these porous materials can be enhanced. Furthermore, there was approximately 40% domain spacing reduction among all samples from the as-cast state to the carbonized state, suggesting a remarkable degree of framework shrinkage under the high temperature pyrolysis step. Notably, MCs derived from Pluronic/resol systems have now been extensively studied and employed in various applications, including but not limited to, energy storage,[87,88] water purification,[89,90] separation membranes,[91,92] photovoltaics,[93,94] capacitors,[95,96] catalyst supports,[97,98] and gas capture.[29,99] Furthermore, this system was extended to the tri-constituent co-assembly of Pluronic/resol/tetraethyl orthosilicate (TEOS) for preparing MCs with enhanced surface area.[100] In this work, polymer-silica and carbon-silica nanocomposites were fabricated through EISA approach, where silica oligomers, resol, and F127 were included into a single solution and assembled together upon evaporation of solvent. Upon calcination and the removal of Pluronic template, domain spacing of MCs only experienced less than 20% shrinkage, which was attributed to the silica inclusions in the nanocomposites strengthening the carbon framework. As a result, this tri-constituent co-assembly method was capable of achieving pore sizes of 8.5 nm and 6.7 nm for the polymer-silica and carbon-silica nanocomposites, respectively. It was also demonstrated that the pore characteristics of these derived mesoporous materials could be manipulated through altering the precursor to template ratio during the synthesis. Moreover, in this system either silica or carbon could be removed from the composite to form single-component mesoporous materials with enhanced surfaced area. One principal advantage of using Pluronic BCPs as the templating agents is that these chemical reagents are all commercially available, providing opportunities for scaled production of MCs to potentially address practical applications. For example, Wang et al. demonstrated a kilogram scale synthesis of MCs using a Pluronic template and resol as the carbon precursor (Figure 3A).[101] In this method, polyurethane foams were acted as macroscopic scaffolds for coating with a resol/Pluronic polymer blend solution (Figure 3B). Through EISA and a post-curing step of resol crosslinking between 100 °C and 180 °C for 24 h, MCs can then be produced after carbonization, which contains uniformly ordered pores around 4.5 nm with surface areas up to 690 m^2/g (Figure 3C). However, there are still several challenges associated with this method, including non-uniform and slow solvent evaporation, limited solution loading content in the foam, and possible carbon yields from polyurethane scaffolds which may result in reduced surface area and porosity of the MCs. Alternatively, a scalable roll-to-roll (R2R) fabrication method was demonstrated to fabricate soft-templated MCs with tunable pore textures by manipulating the solution concentration, material composition, as well as the crosslinking temperature.[102] Specifically, the multi-component solution can be directly cast on polyethylene terephthalate (PET) substrate at an industrially relevant production rate (50 cm/min). After solvent evaporation and thermal crosslinking, the film can be easily released from the substrate, producing free-standing materials for subsequent carbonization process. This R2R method provides a facile route to the scalable production of MCs with comparable material properties and performance from small-batch syntheses.

MCs templated by Pluronic chemicals typically exhibit pore diameter ranging from 4–10 nm, directly related to their domain size from self-assembly. Aiming at obtaining MCs with larger pore sizes (> 10 nm), various research groups studied the use of non-Pluronic polymers as the templates, which often require several steps of custom syntheses.[36,103,104] In many cases, these BCP templates contain a PEO block due to its ability to strongly interact with resol through hydrogen bonding. Several studies employed poly(ethylene oxide)-*block*-polystyrene (PEO-*b*-PS) as the template for MC synthesis,[105-107] which can be prepared by atom transfer radical polymerization (ATRP) and/or reversible-addition-fragmentation chain-transfer (RAFT)

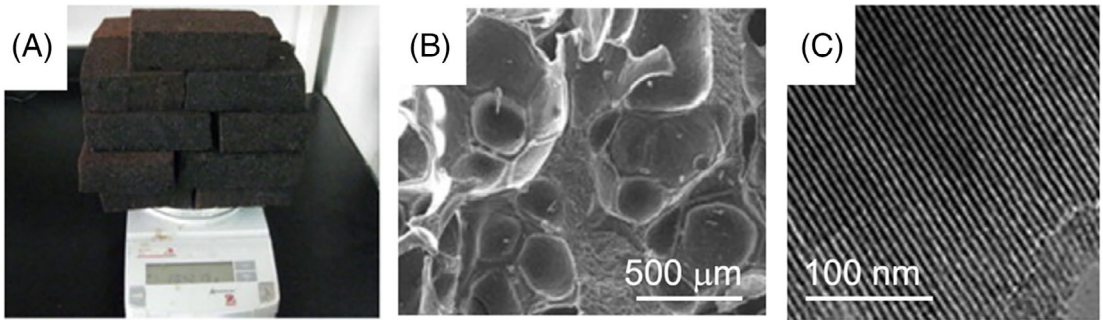

FIGURE 3 (A) Scaled production of MCs using polyurethane foams as scaffolds; (B) the foam can uptake precursor/templating solutions for drying, crosslinking, and carbonization; (C) highly ordered MCs with cylindrical pores can be obtained through this method. Reprinted with permission from Wang et al.[101] Copyright 2011. Elsevier

polymerization method.[108,109] For example, Deng et al. demonstrated the use of PEO-*b*-PS (synthesized by ATRP) as a soft template for MC synthesis, achieving large mesopores up to 22.4 nm in diameter.[110] The synthesis of PEO-*b*-PS was carried out by first functionalizing a PEO homopolymer with bromoisobutiryl bromide to form a PEO-Br macroinitiator. This macroinitiator was then used for chain extension reaction, growing a PS block on the polymer backbone using a copper bromide/pentamethyldiethylenetriamine (PMDETA) catalyst system. The resulting BCP contained PEO and PS constituents with molecular weight of 5700 g/mol and 29,700 g/mol, respectively, and was used as the template for MC synthesis. The ordered, large-size mesopores in these PEO-*b*-PS templated MCs were attributed to the high molecular weight of the hydrophobic PS segments. In another seminal work, MCs with thick walls and large pores were synthesized using poly(ethylene oxide)-*block*-poly(methyl methacrylate) (PEO-*b*-PMMA) as the template,[111] and produced MCs which exhibited face centered cubic close-packed mesostructure with a pore size of approximately 10 nm and wall thickness of approximately 14 nm. The thick pore walls were contributed to the relatively weak association of PMMA block and resol components. Additionally, there are many other reported PEO-based BCP templates for MC synthesis, including but not limited to, poly(ethylene oxide)-*block*-polycaprolactone (PEO-*b*-PCL),[112-114] poly (dimethylsiloxane)-*block*-poly(ethylene oxide) (PDMS-*b*-PEO),[115] poly(ethylene oxide)-*block*-poly(hedral oligomeric silsesquioxane) (PEO-*b*-POSS),[116] polyisoprene-*b*-polystyrene-*block*-poly(ethylene oxide) (PI-*b*-PS-*b*-PEO),[117] and poly(ethylene oxide)-*block*-poly(ethyl acrylate)-*block*-polystyrene (PEO-*b*-PEA-*b*-PS).[118] Notably, it was found that the use of triblock copolymer as the MC template can lead to a broadened processing window to attain the bicontinuous morphology (e.g., gyroid), which is appealing for many applications due to its unique advantage of three-dimensional interconnected pore geometry.[117] Furthermore, there are several studies demonstrating the use of co-templates, namely BCP blends, for producing MCs with hierarchical or multi-phase structures.[105,119] For example, Liu demonstrated a mixed BCP templating system utilizing F127 and PDMS-*b*-PEO as the structure directing agents and resol as the carbon precursor through EISA process.[120] Two templates were cooperatively assembled into hybrid micellar morphologies upon solvent evaporation, where the hydrophobic PDMS segment interacted with the hydrophobic block of the F127 template, consequently swelling the hydrophobic core for increasing the pore size of the resulting MCs.

Furthermore, many studies showed that BCPs without the PEO groups can also be used for soft-templating synthesis of MCs, which their efficient mixing with resol would rely on hydrogen bonding, hydrophilic–hydrophilic and/or ionic interactions. In 2004, Liang et al. demonstrated a polystyrene-*block*-poly(4-vinylpyridine) (PS-*b*-P4VP)/resorcinol-formaldehyde (RF) system for fabricating MCs, through organizing resorcinol-based carbon precursors into P4VP domains driven by hydrogen bonding.[121] The assembled mesostructure was successfully retained during the carbonization step using RF as the precursor, which was crosslinked through the introduction of vapor phase formaldehyde. Specifically, as shown in Figure 4A, assembled PS-*b*-P4VP/resorcinol blend was first prepared in thin films, followed by controlled solvent vapor annealing (SVA) to direct the orientation of the microphase-separated nanostructure. Subsequently, formaldehyde was introduced into a closed-system and locally deposited within the P4VP domain, while polymerizing/crosslinking with resorcinol. After crosslinking and carbonization, MCs templated by PS-*b*-P4VP (this BCP has a less than 1.1 wt% carbon yield) can be obtained (Figure 4B,C). The required use of multi-step process is to overcome the limited mobility of BCPs ordering during the simultaneous RF crosslinking. Similarly, Kosonen et al. designed hierarchical porous carbons with high surface area and

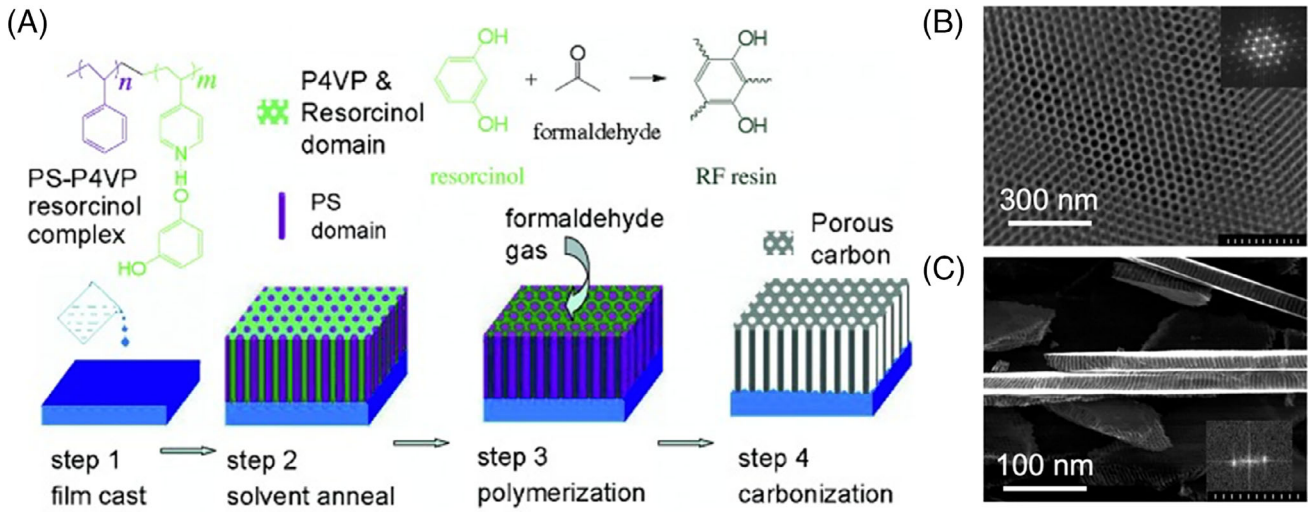

FIGURE 4 (A) Synthesis of MC films using PS-P4VP as the template, and the vapor phase carbon precursor, formaldehyde was introduced for polymerization. (B) After carbonization, these MCs exhibit highly ordered cylindrical structures, (C) which are perpendicular to the film surface.[121] Reprinted with permission from Liang et al.[121] Copyright 2004. John Wiley and Sons

controlled pore size by blending of uncured resol and PS-*b*-P4VP.[122] Favorable interactions between phenolic hydroxyls from the carbon precursor and the pyridine moieties in the BCP through hydrogen bonding resulted in the self-assembly of P4VP/resol surrounding the PS minority domains. After crosslinking with the presence of hexamethylenetetramine (crosslinking agent), the polymer template was decomposed at elevated temperatures resulting in a narrow pore size distribution (averaged pore size ~25 nm) and relatively high surface areas (more than 300 m^2/g). In this study, selectively assembling resol within a phase of the BCP morphologies provided access to multiple pore morphologies including cylinders, spheres, and lamellae, which could be achieved by manipulating the volume fraction of PS in the BCP template. This work provided a versatile method for achieving various pore morphologies by leveraging hydrogen bonding interactions between BCP constituents and carbon precursors. Moreover, ionic interactions can also be used to direct the mixing of carbon precursors and BCP templates, exemplified by the cooperative self-assembly of resol with an unconventional polymer template (poly(styrene-*b*-*N*,*N*-dimethyl-*n*-octadecylamine *p*-styrenesulfonate), (PS-*b*-PSS-DMODA)) prepared by RAFT polymerization.[123,124] However, since this template is composed of blocks with high glass transition temperatures (T_g), the resulting morphology of BCP template/resol composites after crosslinking exhibited very poorly ordered structures. To address this challenge, two different methods were introduced, including (SVA) and the use of non-volatile solvent additives, to improve the degree of ordering for synthesizing MC thin films. The high molecular weight nature of this PS-*b*-PSS-DMODA template resulted in MCs with pore diameters around 20 nm. These studies can be considered as model systems for demonstrating how employing different processing methods provides control over the final MC morphology, which will be covered in detail in the Section 4.2.

2.3 | Block copolymer templates with complex chain topology

In recent years, advances in polymer chemistry enable the synthesis of BCPs containing high complexity in chemical composition (e.g., multiblock copolymers and sequence-defined polymers) and chain architecture (e.g., cyclic and bottlebrush BCPs) through simple and scalable process and with high product yield.[125–127] These breakthroughs also stimulated research interests in employing topologically complex BCPs for the synthesis of MCs, such as some recent works using bottlebrush BCPs as the emerging soft templates. To provide a brief introduction, bottlebrush polymers are branched or graft polymers with polymeric side chains attached to a linear backbone.[128] Due to the steric hindrance from densely grafted side groups, their backbones tend to significantly more disentangled compared to their linear counterparts, leading to unique chain architectures with many properties that are not easily accessible from conventional linear polymers, such as high entanglement molecular weights, fast diffusion constants, reduced energy barrier for assembly and morphological reorganization, and relatively large domain structures (above 50 nm).[129–131] Over the past years, research efforts

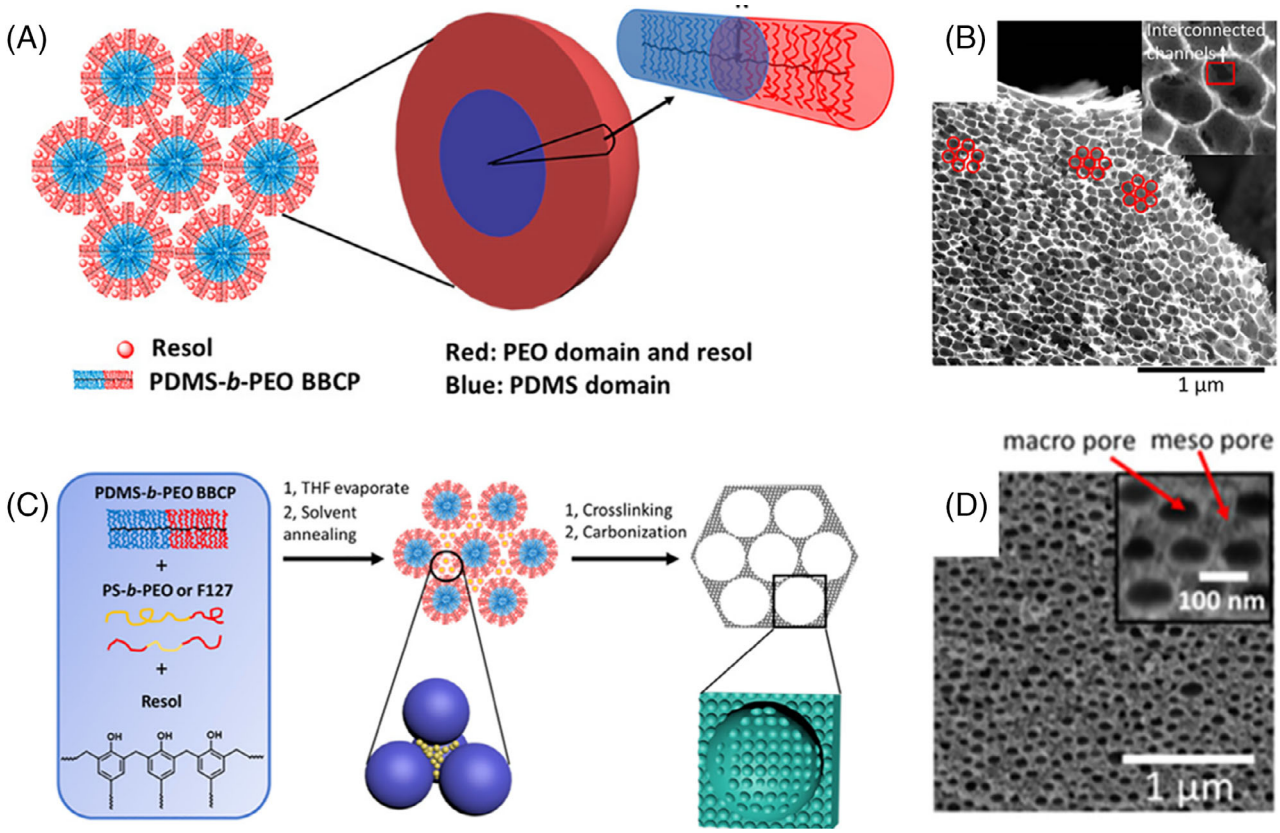

FIGURE 5 (A, B) Cooperative assembly of PDMS-*b*-PEO bottlebrush block copolymer and phenol-formaldehyde resin for preparing large-pore nanoporous carbons.[140] Reprinted with permission from Fei et al.[140] Copyright 2019. American Chemical Society. (C, D) Synthesis of bimodal porous carbon films can be achieved using the mixture of bottlebrush BCP (PDMS-*b*-PEO) and linear BCP (PS-*b*-as the co-templates.[141] Reprinted with permission from Fei et al.[141] Copyright 2020. American Chemical Society

have been focused on exploring the diverse properties, functions, and applications of bottlebrush polymers, demonstrating their potential and promising use in photonic materials,[132,133] nanolithography,[134,135] drug delivery,[136,137] and bio-imaging.[138,139] Regarding their use in MC synthesis, Fei et al.[140] synthesized ordered MC films with tunable pore sizes via co-assembly of a bottlebrush BCP (polydimethylsiloxane-*block*-poly(ethylene oxide) (PDMS-*b*-PEO)) template and resol. The resulting polymer blend films exhibit a sphere-forming morphology (PDMS as the minor domain) with a wide range of feature sizes (diameter of spheres) from 18 to 150 nm, depending on the molecular weight of BCP templates (Figure 5A,B). Upon carbonization, approximately 30% of shrinkage in the nanostructures was observed, leading to the pore size of their derived MC films from 15 nm to 108 nm. The ability of producing such large pores using BCPs as templates was very rarely demonstrated before, and therefore this work not only extended the use of bottlebrush BCPs for synthesizing MCs, but also showed an effective approach to produce large-pore nanoporous carbons. To highlight the advantage of forming large pores in MCs using bottlebrush BCP templates, these nanoporous carbon films were back-filled with vanadium oxide (e.g., V_2O_5) through conformal deposition (without pore blockage) for demonstrating their use in high-performance micro-pseudocapacitors.[142]

Additionally, bottlebrush BCPs can be combined with other linear BCPs to serve as co-templates, yielding hierarchical porous materials with multimodal morphologies. As shown in Figure 5C,D, Fei et al.[141] designed planet-satellite structures of hierarchically ordered bimodal porous carbon films with tunable mesopores by simultaneously employing two different BCP templates, which contains both mesopores (from PS-*b*-PEO, or F127) and macropores (from PDMS-*b*-PEO bottlebrush BCPs), for preparing high-performance supercapacitor electrodes. Particularly, it was observed that size of macropores is tunable within a continuous matrix based upon the selection of bottlebrush template and processing condition, while the mesopores (from linear BCPs) were uniformly surrounded around the macropores. Furthermore, the control over the morphology of these hierarchical, bimodal nanoporous carbons directly dictates their capacitor performance. This co-templating approach can also be extended for the synthesis of porous silica and metal oxides with combined advantages of easy-to-

functionalize pore surfaces, controllable pore morphologies, and high surface areas. In another similar work, PS-*b*-PEO bottlebrush BCPs along with F127 were employed for the production of mesoporous carbons with bimodal pore sizes using dopamine as carbon source.[143] Dopamine and ammonia were included into the micelle (template) solution, resulting in the self-polymerization of carbon precursors surrounding BCP micelles. After carbonization and thermal decomposition of the polymer templates, a bimodal pore size distribution was observed, with averaged pore sizes around 6.5 nm and 24.5 nm. Specifically, bottlebrush BCPs were responsible for the large mesopores and the F127 template corresponded to the small mesopores. This work demonstrated a facile method for the synthesis of bimodal MCs with the ability to broadly access a range of pore sizes and morphologies. Moreover, star-shape polymers and dendrimers can also be utilized in the MC synthesis for obtaining large-pore mesoporous materials.[144,145] For example, Li et al.[114] demonstrated a promising strategy for fabricating a variety of different large-pore mesoporous materials, including carbons, silica, and metal oxides. In this approach, ordered mesoporous resol were templated by poly(ethylene oxide)-*block*-(ε-caprolactone) (PEO-*b*-PCL) blended with a star-shaped poly(ethylene oxide)-functionalized POSS homopolymer. The degree of ordering and pore size of the mesoporous resol after calcination were controlled by varying the template to star homopolymer ratio, as well as the relative POSS concentration in the total solids. Through the inclusion of the star homopolymer, an order-to-order transition, from bicontinuous gyroid to hexagonally packed cylinder morphology, was observed.

3 | DIRECT PYROLYSIS OF BLOCK COPOLYMERS

Soft-templating method for the synthesis of mesoporous carbons has been relatively well-established since their inception, but it often requires efficient mixing of multiple components in the solution state, which can involve large amounts of solvent consumption. In this regard, direct pyrolysis of block copolymers (BCPs) for MC synthesis can provide an alternative method which requires less solvent use, and thus could be more sustainable and energy-saving. As previously discussed, the wealth of different morphologies from BCP self-assembly provides great opportunities to convert these ordered nanostructures into carbonaceous products for different applications. For direct pyrolysis method, a fundamental requirement is that at least one of the BCP components can be efficiently converted to carbon, while the other components should be decomposable for resulting in pores. As most polymers exhibit very low carbon yields, selection of viable precursor materials so far is relatively limited. Particularly, polyacrylonitrile (PAN)-based BCPs are the most common material candidates, in which PAN can undergo a thermal stabilization process at elevated temperatures, allowing their efficient carbonization.[146] Additionally, multiple other examples, such as using photo-crosslinked PS for MC synthesis, have also been reported in the literature which will be covered in this section. Notably, the synthetic rigor, and typically reduced order in mesoporous carbon product from the direct pyrolysis of BCP precursors has resulted in a relatively limited number of studies on establishing order, alignment, and functionalization of these MC systems.

3.1 | PAN-based

PAN-based polymers are commonly used for producing functional carbon materials, including the vast majority being carbon fibers.[147] One of the key advantages of PAN as carbon precursor is its ability to undergo a thermal stabilization process simply through the introduction of heat, resulting in high product yields upon carbonization. The oxidative stabilization typically occurs between 200 °C and 300 °C and consists of multiple different reaction mechanisms that depend on the atmosphere in which the process is performed. The reaction mechanisms and associated kinetics that occur during the stabilization process have been studied in depth through solid state NMR by Liu et al.[148,149] In most cases, thermal stabilization of PAN is performed under air, which the associated reaction mechanisms are depicted by Figure 6. Briefly, the primary mechanism in the initial stage is through dehydrogenation of PAN backbone, forming polyene-like structures. Meanwhile, a secondary, minor reaction can also occur, which is addition of oxygen to the PAN backbone. Both reaction pathways lead to aromatization of the polymer backbones for crosslinking through ring closure of the nitrile units. Additionally, some polyene-like structures in the polymer backbones that were formed in the initial stabilization process may still remain un-crosslinked even after the aromatization step. These reaction pathways can efficiently stabilize PAN for subsequent pyrolysis, allowing it to be converted into carbon materials with a high degree of carbon yield (~50 wt%).

For producing porous carbons using direct pyrolysis approach, it is necessary to include additional components into the PAN backbones for enabling the microphase separation and pore formation. While random copolymers can be potential candidates, they are

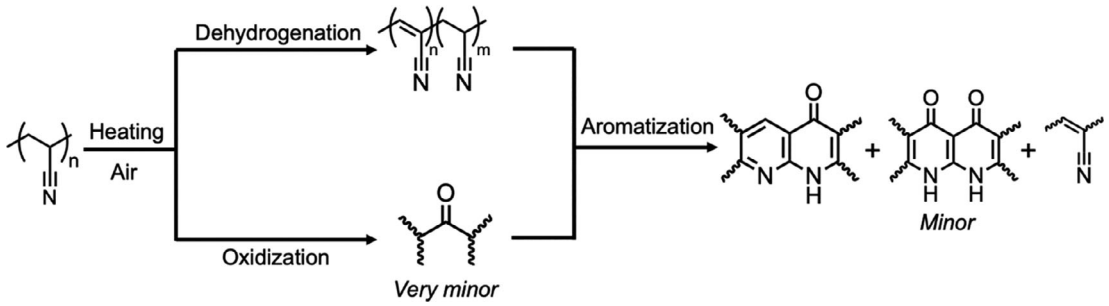

FIGURE 6 Reaction mechanisms that pertain to the oxidative stabilization process of PAN in air. Initially, the polymer backbone undergoes dehydrogenation, forming a polyene structure which is aromatized during later stages of the process

often difficult to yield defined mesostructures upon spontaneous phase separation,[150] which necessitates the use of PAN-based BCPs containing at least one sacrificial minority block as the pore-forming agent for MC synthesis.[151] This has been accomplished using multiple different constituents such as poly(butyl acrylate) (PBA),[152-154] polystyrene (PS),[155] poly(methyl methacrylate) (PMMA),[156-158] and poly(ethylene oxide) (PEO).[159] In general, these polymers were often prepared by controlled radical polymerization methods, such as ATRP and/or RAFT polymerization, which can yield polymers with low polydispersity and controllable molecular weight. In these BCP systems, decomposition of the minority, non-PAN domain resulted in pores, the size of which can be controlled by modulating the molecular weight of the minority constituent of the BCP. Additionally, it is worth noting that the establishment of long-range ordering in the microphase separated PAN-based BCPs can be impeded by the high T_g (approximately at 95 °C) and semicrystalline nature of the PAN, especially when coupled with another high-T_g minority block such as PMMA. In many cases, ordering mobility of PAN-based BCPs could be more limited than their counterparts in soft-templating systems (e.g., during EISA process). Kowalewski et al. demonstrated the use of polyacrylonitrile-*block*-poly(butyl acrylate)-*block*-polyacrylonitrile (PAN-*b*-PBA-*b*-PAN) BCPs for producing thin film arrays of carbon domains,[160] confirming that the ordered nanostructures from self-assembly of PAN-based BCPs can be retained throughout the thermal stabilization and carbonization processes. Since this important work, the concept of directly converting BCPs to MCs has been extended to many different types of polymers for targeting various applications. For instance, Nguyen et al. prepared polyacrylonitrile-*block*-poly(methyl methacrylate) (PAN-*b*-PMMA) through ATRP,[157] which can be self-assembled into ordered hexagonally packed cylinders after slow solvent evaporation from dimethylformamide. After thermal stabilization, the BCP films were directly pyrolyzed, converting the PAN matrix to carbon and selectively decomposing the cylindrical PMMA domains to form mesopores. The resulting carbons exhibited ordered cylindrical pores with surface areas up to 860 m^2/g and an average pore size of 8.1 nm. This pore size was slightly decreased from the cylinder diameter of 12.1 nm from the as-cast BCP films, as determined by small angle X-ray scattering (SAXS). Centering around PAN-based BCPs, the ability to manipulate the size and morphology of the pore textures in their derived MCs has also been intensively investigated. Particularly, as the morphology of self-assembled BCPs is directly determined by the volume fraction of hydrophilic constituents within the system, the resulting MC morphology can be controlled through either physical blending with additional components or post functionalization through synthetic techniques to alter their chemical compositions, which both have been well established. For example, Palanisamy et al. reported that a variety of morphologies, including spherical, worm-like, and lamellar structures in porous carbons could be obtained by simply blending PAN homopolymer with PAN-*b*-PMMA in solution state, to on-demand adjust the volume fraction of total PAN content in the system.[161] Additionally, many works demonstrated the control over the resulting pore morphology in the PAN-derived MCs through synthetic routes, including the synthesis of PAN-containing polymer brushes, and/or controlling the volume fraction of PAN in the synthesized polymers. For example, Yuan et al. synthesized PBA-*b*-PAN polymer brushes with low dispersity side chains through ATRP.[162] Steric hindrance between the bulky, densely grafted side-chains drove the microphase separation, encouraging the formation of ordered mesostructures. After stabilization of the PAN blocks at 280 °C, the BCPs were carbonized, decomposing the PBA domains and producing porous carbons with surface areas up to 420 m^2/g and pore sizes ranging from 4.3 nm – 6.8 nm. Additionally, Wu et al. demonstrated the ability of PAN-grafted PMMA nanoparticles to produce MC.[163] In this work, PMMA nanoparticles were first synthesized which served as both macroinitiators for PAN

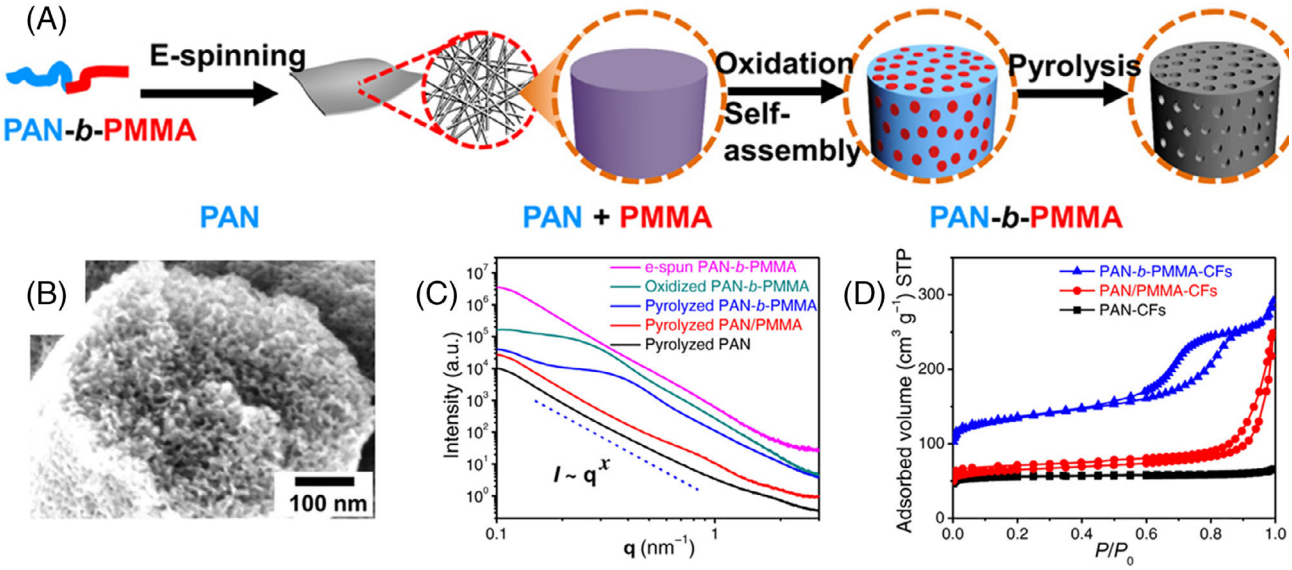

FIGURE 7 (A) Schematic illustration of electrospinning PAN-*b*-PMMA fibers, oxidation of the PAN blocks with simultaneous microphase separation followed by pyrolysis into porous carbon fibers. (B) Scanning electron microscopy (SEM) image of derived MC fibers. (C) SAXS data illustrating ordering of domains in as-spun fibers, oxidized PAN-*b*-PMMA, and pyrolyzed samples. (D) Nitrogen adsorption isotherms comparing porosity in PAN carbon fibers, blended PAN/PMMA carbon fibers, and MC fibers produced from PAN-*b*-PMMA. Reprinted with permission from Zhou et al.[164] Copyright 2019. AAAS

chain extension and the sacrificial, structure-directing template upon carbonization. Upon oxidative stabilization of the continuous PAN matrix, the nanoparticle template was decomposed and mesopores were generated. The carbonization process also introduced microporosity into the carbon framework, increasing the surface area to 487 m^2/g and resulting in bimodal pore sizes of 0.7 nm and 6.8 nm.

Multiple recent works have extended the use of PAN-based BCPs for fabricating mesoporous carbon fibers, showing their high performance for energy and environmental applications. Zhou et al. employed electro-spun PAN-*b*-PMMA as fibral precursors for producing porous carbon fiber (Figure 7).[164] In this work, the polymer fibers were spun into mats, and then exposed to elevated temperatures in air to carry out the crosslinking and thermal stabilization process. As demonstrated in Figure 7C, the as-spun fibers do not exhibit very distinct BCP domains, but microphase separation occurs after oxidative stabilization of the PAN units within the polymer, which may be associated with the increased segregation forces between PAN and PMMA upon crosslinking. The control sample of PAN/PMMA blends does not exhibit any nanoscale ordering, and likely undergo macroscopic phase separation as a result of incompatibility between different homopolymers. This is also evidenced by the nitrogen adsorption isotherms of their carbonized samples in Figure 7D where the type IV hysteresis is present in the PAN-*b*-PMMA derived carbon fibers, corresponding to their mesoporous structures, but such hysteresis is absent in the PAN/PMMA blend or neat PAN carbon fibers. While effective, the resulting carbon fibers only showed a relatively broad primary ordering peak form SAXS measurement, suggesting the limited degree of ordering in their derived MCs. This can be explained by the fact that the self-assembly of PAN-*b*-PMMA occurs during the oxidative stabilization, creating a complex interplay between the increased segregation strength of the PAN/PMMA blocks and the crosslinking reaction restricting the mobility of the polymer chains for ordering. Nevertheless, the BCP-derived fibers in this study exhibited interconnected porous structures with a pore size distribution centered around 9.3 nm and BET surface area of 503 m^2/g. Building on this work, these materials have been employed in a number of different applications, showing their great utility for capacitive deionization,[165] electrochemical applications,[166,167] dye removal for wastewater treatment,[168] and fillers to enhance mechanical properties of nanocomposites.[169]

3.2 | Other nanostructured polymer precursors

While PAN-based BCPs represent the majority of examples in the literature for MC synthesis through directly pyrolyzing BCPs, there are several other examples which utilized distinct chemical components from PANs. These systems typically require additional crosslinking

and thermal stabilization steps for enabling selective materials to become efficient carbon precursors. For example, Yang et al. synthesized BCPs containing poly(vinylidene chloride) (PVDC) as the majority block and poly(acrylic acid) (PAA) as the minority block.[170] Heating the bulk polymer at 200 °C for 1 h prior to carbonization induced dehydrochlorination of the PVDC constituents and the formation of polyene-like structures, similar to those found in the oxidative stabilization of PAN-based systems. The resulting porous carbons upon pyrolysis under nitrogen atmosphere were not highly ordered but exhibited relatively high surface areas ranging from 578 m^2/g to 1093 m^2/g. The pore sizes of these MCs could be manipulated through altering the volume fraction of PAA in the BCP. Aside from inherent crosslinking reactions, multiple studies demonstrated the crosslinking of PS constituents within BCPs can enable the preparation of porous carbons, which usually involve the self-assembly of the BCPs with the inclusion of crosslinking agents. For example, PS can undergo Friedel Crafts hyper-crosslinking in the presence of carbon tetrachloride and a catalyst such as aluminum chloride.[171] Initial works using this crosslinking method focused on PS homopolymers and random copolymers,[172] however, Li et al. synthesized PS-*b*-PMMA BCPs that were assembled into micelles within a mixture of carbon tetrachloride and cyclohexane which served as a preferential solvent for swelling the PS block.[173] Upon introduction of an iron-based catalyst, the swollen PS corona within the micelles can be crosslinked, while the insoluble PMMA core cannot. This resulted in selective degradation of the PMMA domains upon carbonization, forming mesoporous carbon materials with a broad pore size distribution ranging from 2 nm to 170 nm and local maxima at 27 nm and 54 nm. The carbonized products attained surface areas up to 839 m^2/g and exhibited promising performance in supercapacitor applications as well as a high CO_2 adsorption capacity of 5.40 mmol/g at 0 °C. Additionally, multiple works address the fabrication of PS-derived carbon framework in thin film geometries by crosslinking PS segments through the exposure to ultraviolet light at a wavelength of 254 nm. For example, Sun et al. converted PS-*b*-P2VP thin films to MCs through the application of a UV-stabilization process.[174] Specifically, BCP thin films were cast onto a substrate and then exposed to UV light for 2 h, partially crosslinking both PS and P2VP blocks and allowing for their carbonization to occur, for producing carbon films with ordered mesostructures. Importantly, this system required the deposition of a silica mask before carbonization to maintain the morphology and ensure the crosslinked BCP did not decompose during processing. As opposed to the direct pyrolysis of PAN-based BCPs, one of the constituents does not directly act as the sole porogen. Instead, the pore formation occurs from shrinkage, aggregation, and interdomain fusion of the carbon nanostructures. While UV-stabilization of PS segments in BCPs for carbonization has produced mesoporous carbons in multiple instances, the UV crosslinking step is mostly limited to thin film systems due to the limited penetration depth of UV light in bulk systems. Another popular method for the production of MCs is to use polymers which possess high thermal stability without requiring a crosslinking reaction, such as polyimide.[175] For instance, Hatori et al. synthesized MCs through carbonizing poly(ethylene glycol) (PEG) and polyimide blends.[176] The polyimide majority phase only lost 40% of its initial weight upon carbonization, making it an applicable candidate as a carbon precursor. PEG domains within the blends served as sacrificial templates for the generation of pores where it was observed that increasing the amount of poly(ethylene glycol) in the blends improved the mesopore volume of the final carbon product. Additionally, other works have focused on the template-free fabrication of mesoporous carbons through precursors including conjugated polymers,[177] ionic liquids,[178] and others, which have been discussed in detail in some recent reviews.[179]

4 | MORPHOLOGY CONTROL IN ORDERED MESOPOROUS CARBONS

4.1 | Nanostructure ordering mechanisms

Controlling the MC morphology is a central interest in the research community since its degree of ordering and pore texture can directly influence the performance and functionality in various end use. Establishing order in MC systems reduces tortuosity within the pore channels of the material, enhancing diffusion of molecules throughout the carbon matrix. For instance, ion transport ability of ordered cylindrical pores is greatly enhanced compared to disordered worm-like structures of similar size. The improved performance from increased degree of ordering in MCs is also consistent with a number of works describing different applications.[180-182] For MCs derived from hard-templating method, their morphology is inherently constrained to the template (e.g., mesoporous silica).[183] While soft-templating and direct pyrolysis methods enable the facile nanostructure formation through the self-assembly of BCP and/or surfactant, it is also important to note the degree of ordering within these systems can be highly pathway dependent. Particularly, self-assembly is a stochastic process and can be nonergodic.[184-187] Using self-assembled polymers for

fabricating MCs, their attainable nanostructure can be determined by the competition between thermodynamic and kinetic factors. From the thermodynamic perspective, the ordering mechanism of these templating and direct pyrolysis-based systems is identical to the BCP ordering, which is primarily controlled by three key parameters, the Flory-Huggins parameter, the degree of polymerization, and the chemical composition. Readers who are interested in the topic of BCP self-assembly fundamentals can be directed to several excellent articles.[39,73] From the kinetic perspective, the presence of resol (or other carbon precursors) can play a significant role for altering the system mobility in the ordering process of these polymers and their blends. As previously discussed, the use of self-assembled polymers to act as templating agents for MCs is commonly accomplished through EISA. During solvent evaporation, the local concentration of Pluronic BCP significantly increases, resulting in a disorder-to-order transition for microphase separation. Hydrogen bonding between the phenolic moieties in the resol and the PEO block of the Pluronic BCP leads to favorable interactions between template and precursor,[188] strongly assembling the resol oligomers into the PEO domains as well as along the PEO-*b*-PPO interface. Subsequently, resol crosslinking occurs around the PEO matrix upon exposure to elevated temperatures. Multiple works have studied the nanostructural evolution in these systems through various in situ characterization methods. Notably, Florent et al. utilized nitroxide-functionalized surfactants to perform in situ electron paramagnetic resonance (EPR) studies in a model system of Pluronic F127-templated MC, providing some critical molecular level understanding of these processes.[75] Specifically, resol oligomers preferably interact with the PEO domains of the F127 surfactant, however a clear interface between the resol/PEO and PPO domains is not apparent after solvent evaporation. Resol oligomers are pushed towards the micelle corona, forming a distinct interface between the PPO core and PEO shell while also polymerizing around the PEO segments. After establishing the ordered nanostructures, the template can be thermally decomposed through a carbonization step for yielding MCs.

In the case of mesoporous carbon thin films, an alternative mechanism can occur, which is thermal-induced self-assembly (TISA), indicating the phase separation and ordering processes are primarily driven during the thermal crosslinking of resol as opposed to the solvent evaporation. This mechanism was successfully captured by an in situ SAXS study, showing that the introduction of heat induces ordering of F127 or P123 template with the presence of resol.[189,190] As demonstrated in Figure 8, the peak associated with the d-spacing in a film containing hexagonally packed cylinders is not apparent until roughly 20 minutes at 100 °C and reaches the maximum intensity after 2 h of thermal crosslinking. TISA is a result of the segregation strength of Pluronic surfactants being insufficient to induce phase separation between different segments, and as-cast samples only show disordered structures. The segregation strength of a BCP is a function of the interactions between the segments of the BCP, quantified by the Flory-Huggins parameter, and the overall degree of polymerization, where increased degree of polymerization during thermal crosslinking can favor microphase separation. For MC thin films using Pluronic templates, phase separation primarily occurs during resol crosslinking, which is important to drive the segregation forces between distinct components to a sufficient quantity. This phenomenon has also been confirmed for other BCP templating systems, such as PS-*b*-PEO.[191] Additionally, there is often rich interplay between the self-assembly of soft templates and the thermal crosslinking of carbon precursors, which can result in diminished long-range order.[191] At elevated temperatures, the self-assembly kinetics of the BCP template and the kinetics of the crosslinking resin are in competition as resol crosslinking can restrict the mobility of the polymer chains before a highly ordered nanostructure is achieved.

4.2 | Morphology and pore size control

For BCP/resol systems, thermal annealing sometimes is not sufficient because resol crosslinking can significantly hinder the ordering mobility, especially when including BCPs with sluggish ordering kinetics due to their high molecular weight and/or high T_g. Addressing this challenge often requires an additional process step to be implemented in the MC synthesis for the system to establish long range ordering. This is particularly important for preparing MC thin films, which commonly involves rapid solvent evaporation during the film formation.[192,193] In this case, BCP at a highly non-equilibrium state can often be kinetically trapped, resulting in poorly ordered nanostructures. Multiple different annealing methods have been developed to encourage long-range ordering in BCP/carbon precursor thin films and further adapted for use in the production of MC thin films. An early work from Liang et al. utilized SVA to swell a PS-*b*-P2VP thin film which was cast containing resorcinol monomers that selectively were assembled into the P2VP domains.[121] After film formation, it was exposed to a mixture of dimethylformamide and benzene solvent vapors which imparted sufficient chain mobility into the system, allowing for long-range ordered cylindrical domains to be established. The system was then exposed to formaldehyde vapor to polymerize the resorcinol monomers in the P4VP matrix, and subsequently carbonized in an inert atmosphere, selectively decomposing the PS

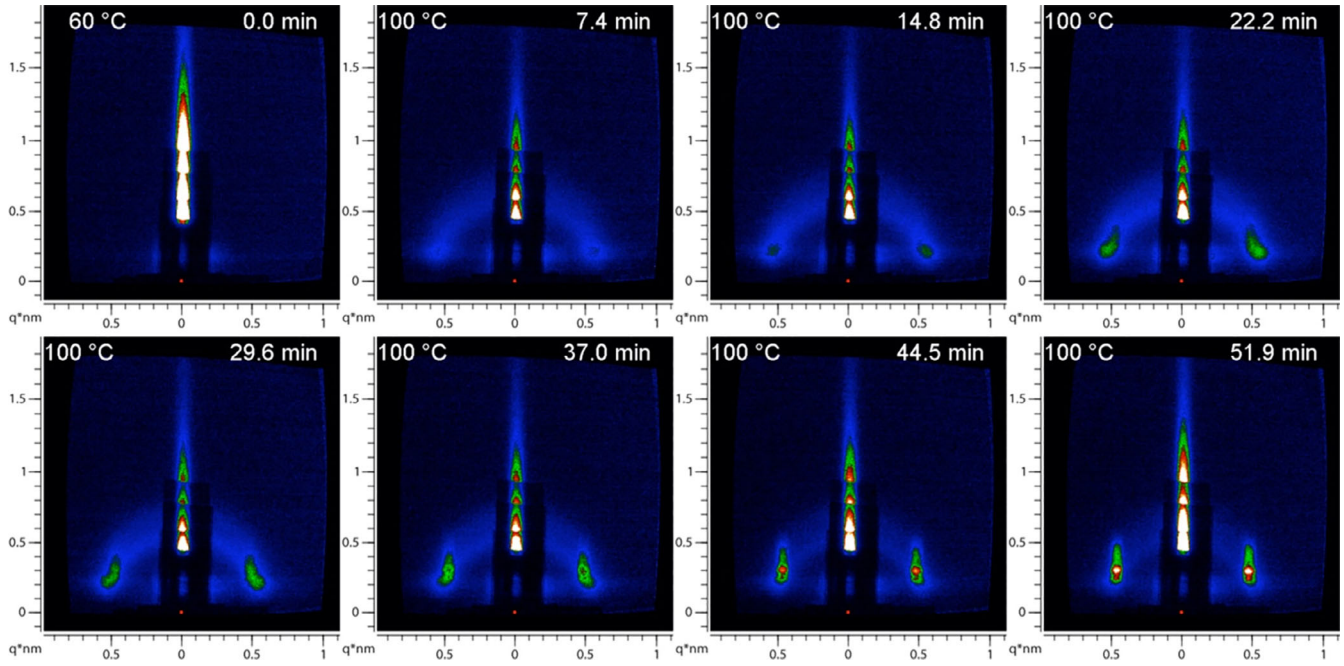

FIGURE 8 In-situ SAXS for demonstrating the formation of ordered microstructure in soft-templated mesoporous carbon thin films using Pluronic BCP as the template and resol as the carbon precursor.[189] The crosslinking temperature is at 100 °C. reprinted with permission from Schuster et al.[189] Copyright 2012. American Chemical Society

domains, and converting the resin into a carbonaceous matrix. This method produced highly ordered pore channels through the entirety of the carbon films that were perpendicularly aligned to the film surface. SVA has also been extended to many other soft-templating systems. For example, the production of MC thin films using PS-*b*-PSS as the template was demonstrated, which the PSS domains can be selectively swollen by resol through electrostatic interactions.[123] After spin-coating, the films were treated with methyl ethyl ketone (MEK) vapor and/or mesityl oxide vapor to induce long range ordering, which was then followed by thermal crosslinking of resol and subsequent carbonization. The solvent vapor annealing conditions, such as relative vapor pressure, could be manipulated to alter the resulting pore size and morphology in the carbon films, and even trigger an order-to-order transition, such as from cylindrical to spherical pores. For example, Deng et al. employed PEO-*b*-PEA-*b*-PS as template, resol as a carbon precursor, and achieved several different nanostructures from a fixed material composition, including a bicontinuous, gyroidal morphology through tuning the processing conditions of solvent vapor annealing, drying/aging, and crosslinking.[194] Using shorter solvent vapor annealing and drying times, gyroid morphologies were achieved, but ultimately transitioned to other morphologies (cylinder or lamellae) upon crosslinking. However, with both longer solvent vapor annealing and drying times, the gyroid morphology could be maintained throughout the crosslinking and carbonization steps. These results further confirmed the existence of a complex interplay between the kinetics of the crosslinking process and the shifting equilibrium as resol crosslinks. Alternatively, it was also found that the introduction of solvent additives, those having low volatility, can also efficiently order the BCP/resol films, which the residual high boiling point solvents in the films can impart BCP chain mobility for ordering during resol thermal crosslinking. Specifically, Qiang et al. used a PS-*b*-PSS BCP to fabricate MC thin films through the introduction of selective solvents into the casting solutions.[124] Dimethyl sulfoxide (DMSO) and dioctyl phthalate (DOP) were added into the casting solution as selective solvents for the hydrophilic and hydrophobic blocks, respectively. Increasing the loading amount of additives in the casting solution enhanced the degree of ordering of the template/resol films after thermal crosslinking, but resulted in dewetting of the polymer film at additive concentrations greater than 25 wt% with respect to solids. Additionally, increasing DMSO and DOP content in the casting solution resulted in shifts towards larger pore sizes of MC thin films, from 3.1 nm with no additives, up to 9.9 nm with 20 wt% in the casting solution due to swelling of the BCP domains. This method has been demonstrated in multiple soft-templated MC systems and is potentially industrially viable for manipulating the structures in fabricated carbon thin films.

Pore size of MCs is an important material parameter for many practical applications, especially those related

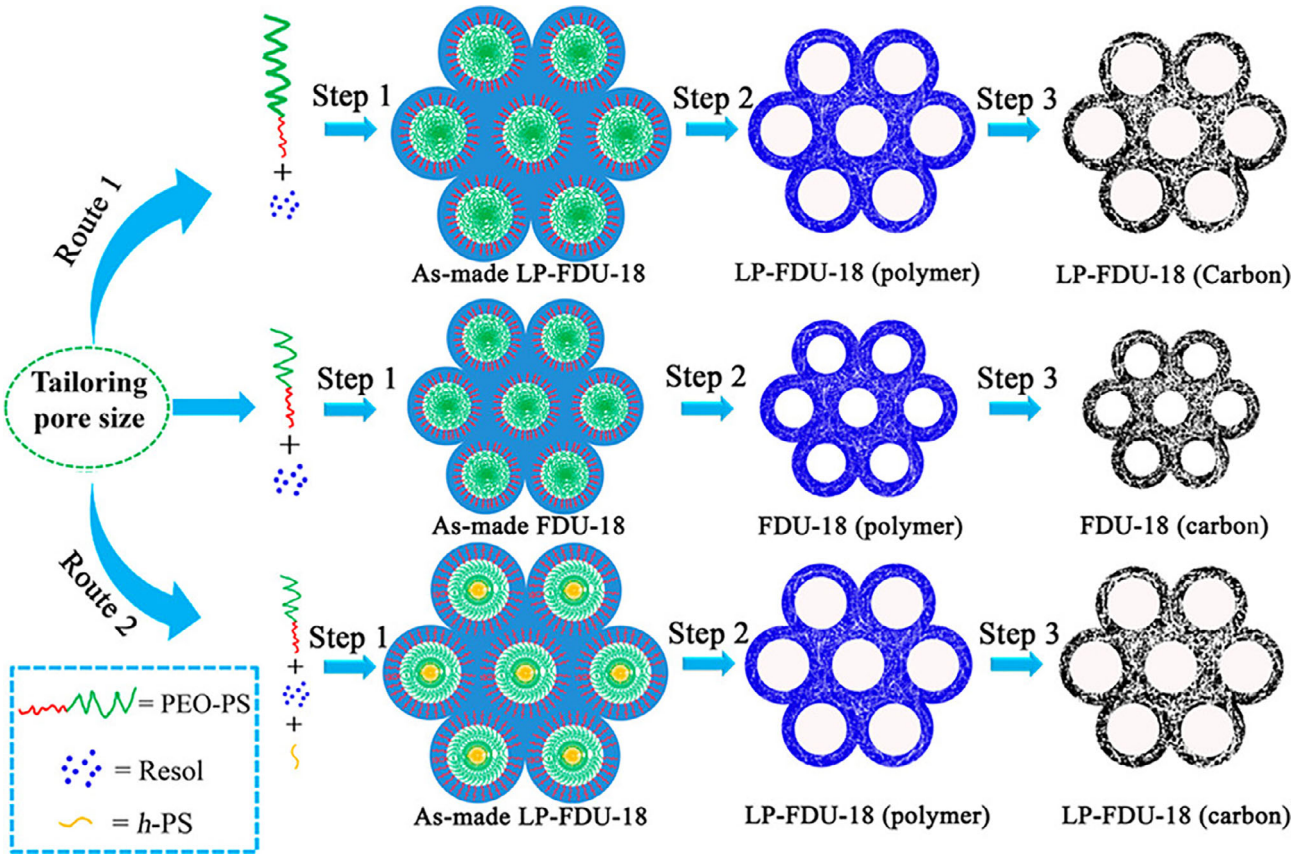

FIGURE 9 Preparation of large-pore mesoporous carbon FDU-18 (LP-FDU-18) polymer and carbon via two approaches: (1) increasing the molecular weight of the hydrophobic segment (PS) of the block copolymer (PEO-*b*-PS) and (2) adding hydrophobic homopolymer (*h*-PS) to the micelles of the block copolymer (PEO-*b*-PS). (step 1) co-assembly of resol and block copolymer template. (step 2) calcination at a low temperature to eliminate the template. (step 3) carbonization at a high temperature to finally obtain ordered mesoporous carbon.[196] Reprinted with permission from Wei et al.[196] Copyright 2017. American Chemical Society

with transport and sorption of guest molecules within pore channels. As discussed in the previous sections, the self-assembly of commercial Pluronic BCPs and resol via EISA method can only fabricate MCs with pore sizes usually below 10 nm.[88,195] As a direct comparison, MC prepared by using PEO-*b*-PS (molecular weight: 29,700 g/mol) as the template exhibited a significantly larger pore size of 22.6 nm, confirming that increasing the molecular weight of the hydrophobic segment (PS) of the BCP template and/or precursors is an effective approach to create large mesopores in the resulting MC products (Figure 9, route 1).[196] Specifically, when the molecular weight of PS segment in BCP template increased from 12 to 30.5 kg/mol, MCs showed an improved averaged pore size from 11.9 to 33.3 nm.[105] Alternatively, using pore expanders for selectively swelling hydrophobic domains can also lead to enlarged pore sizes of MCs (Figure 9, route 2), which can be advantageous as it may not require custom and/or sophisticated syntheses. This concept was initially demonstrated in the preparation of large-pore mesoporous silica, which hydrophobic solvents can be incorporated into Pluronic or CTAB-based templates for increasing the size of hydrophobic cores.[197] However, this method of pore swelling is only applicable for the template/precursor assembly in aqueous solution systems as organic solvents would be easily evaporated during the EISA process for synthesizing MCs. Therefore, hydrophobic homopolymers (such as PS) are employed as the pore expanders to swell the hydrophobic domains by blending them with polymer templates in the system.[198] For instance, adding 0 to 20 wt% of PS with molecular weight of ~9400 g/mol relative to PEO-*b*-PS enlarged the pore size from 22.9 to 37.4 nm of final MC products. Additionally, several studies demonstrated other efficient strategies for increasing the pore size of MCs with low volatile solvents. For example, Trivedi et al.[199] successfully modulated both expansion and contraction of the cylindrical mesopores within MCs, fabricated from the assembly of Pluronic F127, resol, and TEOS, using four different low-volatile solvents. This was achieved by understanding the Hansen solubility parameters between polymer templates and different solvent additives, which allows the use of

quantifiable octanol–water partition coefficient (K_{ow}) to effectively control the pore size in cooperatively assembled mesoporous materials. Specifically, glycerol triacetate (with K_{ow} of less than 1) reduced the pore size from 5.9 to 4.8 nm due to reduced chain stretching of F127 template, while both trimethyl benzene (with K_{ow} of 3.42) and dioctyl phthalate (with K_{ow} of 8.1) can increase the pore size to 8.1 and 13.5 nm, respectively. Moreover, a more hydrophobic solvent, tris (2-ethylhexyl) trimellitate (with K_{ow} of 12.5), was less effective in increasing the pore size (up to 8.2 nm). This study demonstrated a facile route for manipulating the pore size of MCs using solvent additives as the swelling agents with precise and on-demand control. Furthermore, applying carbon dioxide with varied system pressure during synthesis has also been used to modulate pore diameters and surface areas of ordered mesoporous silica. For instance, Hanrahan et al.[199] demonstrated a controllable pore expansion within mesoporous silica using supercritical carbon dioxide, which a controlled swelling of the polymer templates with a maximum pore expansion of 54% was achieved at a pressure of about 482 bar. However, such method has not yet been established in the MC systems for controlling their pore size to the best of our knowledge.

Moreover, altering processing conditions for ordering BCP/carbon precursors can also affect the resulting pore size and structures of MCs. Using BCP assembly as a reference, it is known that the degree of ordering may influence the domain spacings of their derived patterns, and similar relationship was also observed for MC systems.[196,199,201] For example, it has been demonstrated that improved long-range ordering in MC thin films templated by PS-*b*-PSS-DMODA films also resulted in an expansion of pore size by ~40%, compared to their counterpart without SVA treatment.[123] Similarly, Zhou et al. fabricated MC films from a PAN-*b*-PMMA BCP and found that increasing the thermal annealing temperature from 100 °C to 300 °C resulted in varied pore sizes.[158] Annealing at 100 °C resulted in a mostly disordered structure with pore sizes of roughly 40 nm which became ordered at temperatures above the T_g of the PAN blocks, leading to an increased pore size of 50 nm.

4.3 | Directional pore channels through alignment

Producing aligned pores in MCs is highly desired for multiple applications especially those demanding fast and unidirectional diffusion of guest molecular species within pore channels, primarily due to two advantages.[40] First, alignment of nanodomains can minimize the tortuosity of diffusion pathways, facilitating the transport of species and enabling faster sorption/diffusion kinetics. Additionally, MCs with unidirectional nanostructures can exhibit enhanced material properties along the alignment direction compared to their random-oriented analogues. For example, aligned pore channels can greatly enhance the performance of carbon-based electrochemical sensors.[201] Specifically, through formation of aligned pore channels, MC films as electrochemical sensors can achieve an ultralow detection limit (~50 nmol L^{-1}) with a very high sensitivity for dopamine detection. In general, the alignment of nanostructures is often achieved by engineering BCPs and/or their blends containing carbon precursors prior to the thermal crosslinking and carbonization steps. It is important to note that while the direct pyrolysis of BCPs has been used to synthesize mesoporous carbon materials, most of these works rely on PAN-based copolymers which are semi-crystalline. BCP with PAN as majority phase has been very challenging to establish highlyordered nanostructure and unidirectional alignment due to hindered chain mobility, and methods for establishing aligned pore channels in these systems are still largely underdeveloped. However, many approaches have been developed to enable directional alignment of pore channels in soft-templating based systems, most applying on two-dimensional MC films, including both parallel and perpendicular to the planar direction. As an example, SVA can be combined with the application of shear forces to align soft-templated systems prior to crosslinking.[202] In this method (Figure 10A), shear force was deployed through the simple application of an elastomeric pad on the surface of the BCP/resol blend film during solvent vapor annealing.[203,204] Upon exposure to the solvent vapor, BCP/resol film can be swollen, introducing sufficient mobility to the BCP template to induce long range order. As the elastomer dries, it contracts across the surface of the templated film, effectively applying a shear force for aligning the ordered domains. This approach has been first established for neat BCPs with different molecular weight and chemical compositions. As shown in Figure 10B, successful alignment of nanodomains in MCs resulted in a high Herman's orientation factor of the cylindrical mesoporous carbon thin films ($S = 0.88$). It was also found that due to the highly aligned morphology, the conductivity of MCs greatly increased (~40%) in the direction parallel to the pore channels compared to the perpendicular direction (Figure 10C).

Furthermore, zone annealing method was also employed for aligning the Pluronic-templated MC thin films.[205,206] To provide a succinct background, zone annealing is a technique that was initially developed to remove crystal defects in high-purity metals and semiconducting materials,[207] which has also been used to induce highly aligned BCP domains both with and

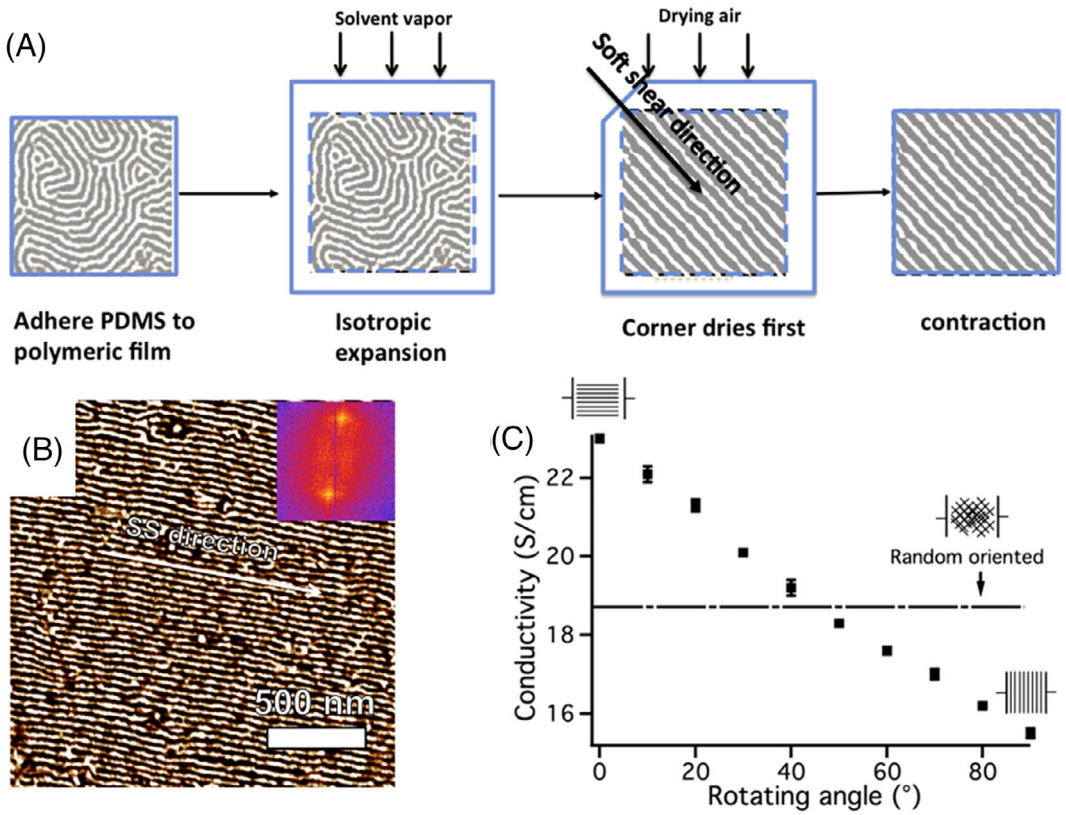

FIGURE 10 (A) Schematic illustration of SVA with soft shear method for aligning BCP/resol films. (B) AFM phase image of a cylindrical forming PEO-*b*-PBA/resol film after carbonization. The solvent used in both cases was tetrahydrofuran. Insets demonstrate the corresponding fast Fourier transform (FFT) diffractograms. (C) Conductivity of aligned mesoporous carbon films a function of the orientation of the electrodes to the alignment direction of the cylindrical mesopores.[202] Reprinted with permission from Qiang et al.[202] Copyright 2015. Elsevier

without the presence of a soft elastomer capping on the top of polymer thin films.[208-211] In zone annealing, a thin film is passed through a thermal gradient and induces rapid orientation of microdomains at the moving front between the hot and cold regions. Xue et al. demonstrated that zone annealing can align the self-assembled domains in thin films from both Pluronic P123 and F127 templates with the presence of resol oligomers.[205] The resulting cylindrical morphologies were aligned in-plane to the film surface and stabilized during the crosslinking of the resol oligomer, allowing them to be maintained after carbonization. It is important to note that the success of zone annealing process depends upon the mobility or viscosity of the template. P123, having a much lower viscosity than F127, could be aligned through zone annealing to ultimately result in mesoporous carbon films with an orientation factor of 0.98.[205] Films templated by higher viscosity F127 only achieved an orientation factor of 0.48 due to reduced mobility during the annealing process. Notably, Tang et al. demonstrated a similar technique for aligning lamellar domains of a PAN-*b*-PBA BCP along the direction that is normal to the film surface (out-of-plane) through zone casting.[212] Zone casting is similar to zone annealing but involves casting a film onto a moving surface; rather than the orientation of microdomains forming along a moving thermal front, it occurs along the front of solvent evaporation as the film is cast.[212] Both techniques have produced highly aligned MC films, which can be potentially scalable, such as when combined with large-scale R2R processes for manufacturing industrially viable products.[213] Flow-induced alignment of nanodomains was also demonstrated in several other reports for the fabrication of anisotropic MCs. For example, Wu et al. demonstrated the ability to orient pore channels within mesoporous carbon films through exposure to air flows.[214] Resol and P123 were combined together in solution, and then deposited onto silicon substrates and exposed to a stream of hot air (80 °C) for 20 s. The shear force and rapid evaporation of solvent caused by the hot air stream resulted in highly aligned templates with morphologies that can be retained through the carbonization process. Moreover, a recent work (Figure 11) utilized an F127 soft-template, dopamine as a carbon precursor, and benzene as a

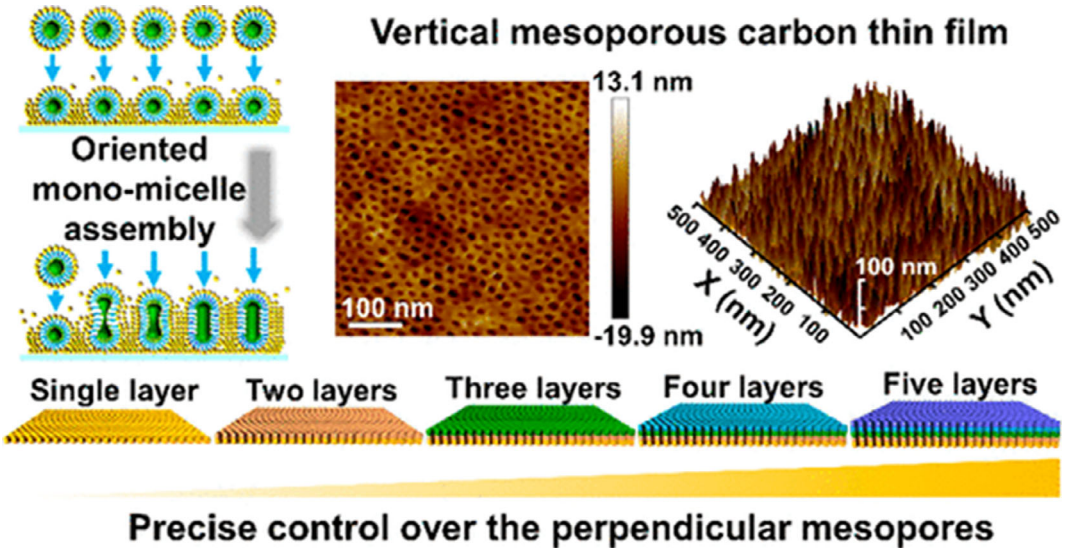

FIGURE 11 Schematic illustration of the self-assembly in a soft- templated mesoporous carbon thin film system which uses polydopamine as the carbon precursor.[201] Initially, composite micelles are formed, and then packed onto a substrate. Benzene additives swell the individual micelles and fuse them together to form rod-like channels. As the carbon precursor is polymerized and carbonized, the rod-like micelles serve as a template for directional pore channels. Reprinted with permission from Wang et al.[201] Copyright 2021. American Chemical Society

swelling agent to both swell and fuse micellar domains into directionally aligned channels prior to carbonization.[201] The resulting MC films exhibited highly aligned cylindrical pores across a range of thicknesses, with pore sizes ranging from 8.4 nm to 13.5 nm, and the alignment of the pore channels throughout the film thicknesses exhibited enhanced performance as electrochemical sensors.

5 | MC FUNCTIONALIZATION

While MCs have found important use in many applications, their properties and performance can be further enhanced through various functionalization methods, including activation for improving porosity and surface area, doping carbon framework through introducing heteroatoms, and inclusion of nanoparticles within the carbon matrix. For example, including nitrogen atoms within the carbon framework can be beneficial for improving the performance of materials in electrochemical oxygen reduction reactions.[215,216] Additionally, sulfur-doped carbon materials have a variety of potential applications including water treatment.[217,218] These important strategies can be effectively combined with nanostructured polymer derived MCs. In this section, we will discuss methods for increasing surface areas of MCs through activation, various techniques for including heteroatoms into carbon products, and other methods of functionalizing MCs such as graphitization and incorporating metal nanoparticles.

5.1 | Activation

MCs templated by surfactant and/or BCP typically exhibit surface areas in the range of 300–600 m^2/g, while direct pyrolysis of BCPs often yields lower surface areas (less than 250 m^2/g). However, many MC applications would require materials to have high surface area for enhanced sorption/reaction sites and behaviors, such as water purification,[219,220] CO_2 adsorption,[29,221] hydrogen storage,[222,223] and supercapacitors.[224,225] In Section 2.2, we discussed that that the cooperative assembly of TEOS, resol, and Pluronic BCP can yield high surface area MCs (up to 2100 m^2/g) after the removal of silica particles from the carbon framework by an etching step using acidic/basic solutions. Another very common strategy for enhancing the surface area of porous carbons is through chemical activation, which creates micropores within the carbon matrix, thus increasing the surface sites (micropores) available for interaction and sorption with external species. In general, activation process can be achieved through the use of different chemical reagents, such as potassium hydroxide (KOH), CO_2, and water vapor, which can selectively react with carbon and remove portions of it from the framework. In the case of using KOH as an activating agent, carbon

framework can be partially etched through the following reaction,

$$6KOH + 2C \rightarrow 2K + 3H_2 + 2K_2CO_3.$$

Briefly, KOH activation can be conducted by physical blending of activation agents with carbons, followed by subsequent exposure to high temperatures (>700 °C) in an inert atmosphere. In this process, optimization of the activation condition is important for attaining maximized surface area without inducing structural collapse of the ordered structures in MCs.

Lv et al. performed a comprehensive study on understanding how the activation reaction conditions impact pore size, surface area, and the degree of ordering of MCs, by investigating both activation time and KOH/carbon ratio using Pluronic-templated carbons as a model system.[224] In this work, it was demonstrated through SAXS experiments that the ordering of the cylindrical pore structures was maintained across all activation conditions. However, the effect of activation on the pore textures varied according to different conditions, such as the KOH to carbon mass ratio. At high ratios (e.g., KOH: MC = 6:1), a large amount of micropores were generated after 45 min, increasing the surface area of MC from 660 m^2/g to 1280 m^2/g. Optimized surface area (~1400 m^2/g) were achieved at 60 min of activation time, while further extending activation time resulted in carbon framework shrinkage and reduction of the surface area (1200 m^2/g) due to the generation of too many micropores for downgrading the mechanical integrity of carbon walls. While activation at these high KOH: MC concentrations can greatly enhance the surface area through the introduction of micropores, the generated pore sizes upon this reaction could be too small (<1 nm) to access for many practical applications. To address this challenge, it was found that at a KOH/carbon ratio of 1 and activation time of 90 min, active potassium species would aggregate in the micropores of the carbon framework, resulting in the formation of a hierarchical network of interconnected micropores and mesopores with an enhanced surface area of 1410 m^2/g, which is particularly advantageous for electrochemical applications such as supercapacitors. This KOH-based activation process has been employed in numerous works as a simple and cost-effective method for increasing the surface area of MCs. Additionally, CO_2 or steam gas can also be used for carbon activation at high temperatures. In the case of CO_2 activation, MCs can be heated at temperatures greater than 900 °C in an inert atmosphere, and then CO_2 can be purged into the system for a desired amount of time. This process generates micropores in the carbon framework, while surface area of resulting activated MCs can be optimized through changing the activation time and/or temperature. An early work from Xia et al. described the impact of activation time on the MC structure using a model system, showing that increasing activation time can result in the generation of micropores to a significant extent that may disrupt the degree of ordering within their mesostructures.[226] However, intermediate exposures at 950 °C resulted in both enhanced surface areas and pore volumes which were key in improving the hydrogen storage capacity of MCs. Similarly, water vapor at high temperatures can generate micropores in carbon materials. As an example, Ludwinowicz et al. performed a study which covered several different activation processes, including steam activation, on the effect of surface areas of pore structures in commercially available, polymer-derived ordered mesoporous carbons.[227] This work found that KOH activation of the commercial product (570 m^2/g) was the most effective in terms of generating microporosity and enhanced surface areas (2030 m^2/g), while CO_2 (1680 m^2/g) and steam activation (810 m^2/g) were found to be less effective.

5.2 | Doping

Generally, introduction of heteroatoms, such as oxygen, nitrogen, sulfur, boron, and phosphorous species, into the carbon matrix can lead to enhanced material performance. For instance, incorporating nitrogen groups in the carbon framework can enhance the CO_2 adsorption capacity of MC sorbents due to favorable interactions between the gas molecules and nitrogen sites. In addition to carbon capture technologies, doping heteroatoms into carbons can also be advantageous for oxygen reduction reactions,[228,229] metal-sulfur battery,[230,231] hydrogen storage,[232,233] and pollutants removal from water,[234,235] all relying on altering the electronic band structure of carbon materials for improved sorption and/or reactivity. Doping carbons is commonly achieved through two different strategies, including 1) directly using precursors which contain heteroatoms and can be stabilized within the carbon framework and 2) reacting carbon precursors with heteroatom-rich chemicals for performing in-situ doping reactions during/after pyrolysis. In general, heteroatom-containing molecules can be used as precursors in both soft-templating and direct pyrolysis methods to incorporate heteroatoms into the MC products but are often limited to synthesizing nitrogen and sulfur doped carbon materials. For instance, melamine resins,[236] polypyrrole,[237] and PAN based systems have all been demonstrated in the literature as efficient carbon source which successfully impart nitrogen heteroatoms at

moderate levels (up to 12 wt%).[238] Additionally, some works have shown the successful conversion of sulfur and nitrogen containing ionic liquids into nitrogen and sulfur co-doped carbon,[239] as well as the use of polythiophene-based polymers for producing sulfur-doped carbons.[240] While these precursors can effectively retain the associated heteroatoms in the resulting carbon framework, the use of boron and/or phosphorous-containing carbon precursor for producing corresponding doped MCs is still underexplored. Alternatively, utilization of heteroatom containing reactants can result in carbons that are doped with different heteroatoms and a controllable doping content. For example, early work in this area involves the use of ammonia gas for producing N-doped MCs. Wang et al. synthesized MCs using F127 as the template and resol as the carbon precursor.[241] After EISA, the templated resol was carbonized in the presence of gaseous ammonia, ultimately doping the final product with up to 9.3 wt% nitrogen in the carbon framework. This chemical process also activated the carbon, reaching surface areas of ~1400 m^2/g and exhibited elevated capacitance in applications as double-layer capacitors. Similarly, it has also been demonstrated that exposure to fuming sulfuric acid vapor for extended periods of time could effectively functionalize MCs for sulfur doping, which Xing et al. used this method for preparing MCs with 1.2 wt% sulfur, enabling their advanced performance of high selectivity and stability in catalysis applications.[242] In addition to gas phase doping strategies, heteroatom-containing dopants can be physically blended with carbon precursors, which heteroatoms can then be effectively introduced into the carbon matrix at different processing stages. For instance, Xue et al. synthesized phosphorus-doped mesoporous carbons by including phosphoric acid into solutions with F127 templates and resol carbon precursors.[243] Films were cast onto substrates, and the phosphoric acid assembled with resol oligomers through EISA. This method was able to produce phosphorus-doped carbon with up to 5.6 wt% phosphorus, but elevated phosphorus loadings adversely impacted the pore characteristics of the material. The neat MCs exhibited surface areas of 588 m^2/g and pore sizes of 3.1 nm, which were maintained until the phosphorus loading levels exceeded 1.7 wt%. At higher doping content, the ordered mesostructured was disrupted. This work also showed that doping phosphorus into the framework of these carbon materials can enhance their performance in electrocatalytic applications.

In another seminal work, nitrogen, sulfur, phosphorous, and boron doped MCs were successfully synthesized using melamine, benzyl disulfide, ammonium dihydrogen phosphate, and boric anhydride as the heteroatom precursors, respectively, combined with a "melting-diffusion" based doping method as shown in Figure 12.[244] Specifically, an ordered mesoporous silica-polymer composite was first prepared, which was then physically mixed with aforementioned dopants. Notably, this strategy decoupled the self-assembly process of carbon precursor with the template and the introduction of heteroatom species into the system, resulting in high degrees of heteroatom content, of which doping content could be manipulated through simply altering the ratios at which the precursors were mixed. This method is able to produce MC with up to 26.3 at%, 15.5 at%, 6.9 at%, and 4.2 at% of nitrogen, boron, phosphorus, and sulfur, respectively, while maintaining the relatively well-defined mesopores and high surface areas. Using this strategy, it has also been demonstrated that co-doped MCs, which contains two or more different heteroatoms, can be prepared by using multiple dopants for simultaneous doping reactions.[245]

5.3 | Others

In addition to activation and including heteroatoms into MCs, there are multiple other methods for enhancing their performance aiming to address various advanced applications. For example, inclusion of metal and/or metal oxide nanoparticles into mesoporous carbons can be very useful for a broad range of different applications, such as catalyst,[246] energy storage,[247] and water remediation.[248] Generally, this can be accomplished through the use of various metal nitrate precursors that are easily dissolved in resol/BCP template solutions for cooperative assembly, resulting in the introduction of different nanoparticles in MCs. This includes but is not limited to, nickel,[88,249] iron oxide,[250] cobalt oxide,[106] and zinc oxide.[251] For instance, García et al. fabricated mesoporous carbon-nickel nanoparticle composites by heating a solution of nickel (II) nitrate hexahydrate, P123, resorcinol, and formaldehyde in an autoclave for 4 days in acidic conditions.[252] During this process, the nickel precursor and resorcinol-formaldehyde oligomer can be self-assembled within the hydrophilic micelle coronas due to hydrogen bonding. The samples were then crosslinked and carbonized. It was found that increasing the loading levels of metal nanoparticles resulted in decreased surface areas (from 730 m^2/g for neat carbon to 390 m^2/g for 6.5% nickel loadings), while the pore sizes was maintained around 6 nm. The ordered structures in MCs were also retained and the metal nanoparticles, ranging from 10 nm – 50 nm in diameter, can be well dispersed in the matrix. Similarly, Wang et al. fabricated carbon-cobalt oxide nanocomposites through a similar co-assembly method using cobalt

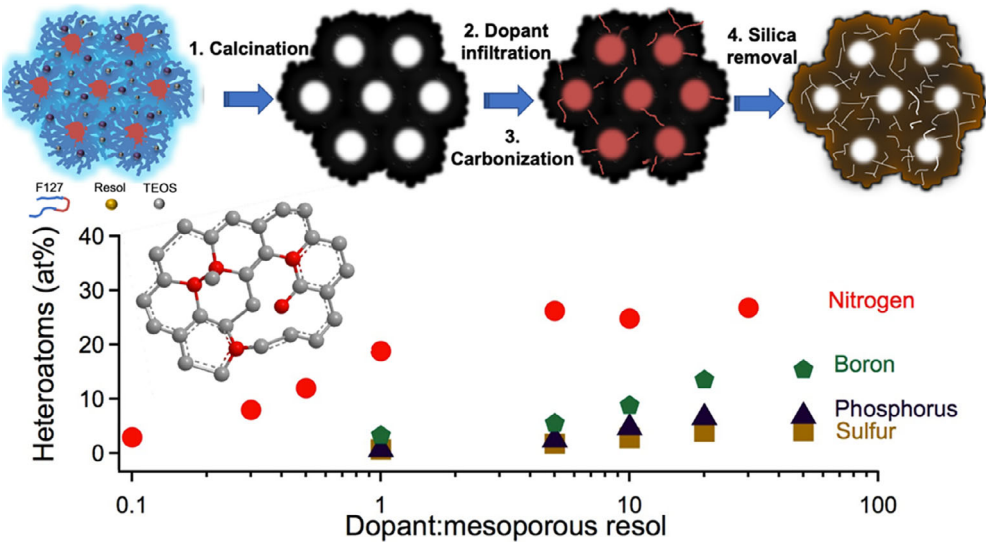

FIGURE 12 Schematic illustration of melt-diffusion doping strategy to produce heteroatom-doped MCs with controllable doping content by adjusting the mass ratio of dopant and mesoporous resol. This method includes steps of cooperative assembly, calcination to generate mesoporous polymer−silica, the melt diffusion of dopants for their infiltrating into pore channels, and subsequent carbonization. Reprinted with permission from Qiang et al.[244] Copyright 2017. American Chemical Society

nitrate hexahydrate as a metal nanoparticle precursor, a PEO-*b*-PS template, and resol as the carbon precursor.[106] The carbon-metal nanoparticle composites had uniform pore sizes in the range of 13.4 nm to 16 nm and achieved surface areas up to 483 m^2/g. The high molecular weight PEO-*b*-PS template resulted in large pore sizes and thick pore walls, which were vital in nucleation and stabilization of the metal nanoparticles. This MC/cobalt oxide nanocomposites showed great potential in H_2 sensing applications. This strategy of introducing functional nanoparticles in MCs through cooperative assembly of precursor/template/metal nitrates and can be extended to large-scale (gram to kilogram) production of nitrogen-doped, mesoporous carbon-iron oxide nanocomposites.[253] In this work, a solution of resol, P123, dicyandiamide, TEOS, and iron nitrate was deposited onto PET substrates through a R2R processing method. Resol and P123 acted as the carbon source and template, while dicyandiamide, iron nitrate, and TEOS acted as a nitrogen source, iron source, and silica source, respectively. All components within the system can be successfully assembled into ordered nanostructures. After carbonization, the silica within the carbon framework was etched to generate micropores and increase surface areas. The introduction of the nitrogen heteroatoms and iron nanoparticles reduced the surface areas of the MC from 2160 m^2/g to 1100 m^2/g for 10.8 wt% iron nanoparticles and 970 m^2/g for 21 wt% iron nanoparticles as a result of the nanoparticle crystallization disrupting their ordered mesostructures. Despite the reduced surface areas, the nanocomposites exhibited excellent cycle stability as anodes for sodium-ion batteries with nearly 99% capacity retention after 350 cycles.

Another noteworthy method for further enhancing the properties of MCs is through enhancing the graphitization degree of their carbon walls, especially since many MCs applications would demand excellent conductivity, thermal stability, and mechanical strength. The attained degree of graphitization of carbons upon pyrolysis is often dependent on the precursor selection. In systems such as PAN-derived carbon fibers, graphitization is accomplished by exposure to very high temperatures (>2000 °C), which is very energy intensive.[254] For MCs that commonly used resol as the precursor, many approaches have been established for achieving enhanced graphitization of carbon walls, such as including catalyzing graphitization through nanoparticles and using more easily graphitizable precursors. It has been demonstrated that the inclusion of transition metal nanoparticles can assist in reducing the energy required for inducing graphitization of resol-based ordered mesoporous carbon. Tang et al. studied the effect of co-assembling tungsten (W), molybdenum (Mo), and titanium (Ti) salts with a P123 soft template and resol on the graphitization of the resulting carbons.[255] Generally, the introduction of these nanoparticles maintained the surface area of the porous carbons (~550 m^2/g) but greatly improved the degree of graphitization after carbonization at 700 °C for 2 h. The ratio of the intensities of the D-band (1360 cm^{-1}) and G-band (1590 cm^{-1}) (I_D/I_G) in the Raman spectrum indicates the degree of graphitization of the carbon material, where lower ratios correspond to higher amounts of

graphitized carbon relative to disordered carbon within the system. Introducing transition metals into the carbon matrix reduced the I_D/I_G of the carbon materials from 1.596 to 1.540, 1.413, and 1.340 for the Ti, Mo, and W inclusions, respectively. This highlights the capability of these metals to greatly facilitate the graphitization process of carbons through a simple co-assembly approach. Increasing the graphitic character in MCs can also be achieved through the introduction of other non-catalytic components in the cooperative assembly process. Beitollahi et al. produced highly graphitic carbons through including trihydroxyanthraquinone, tetracycline, and 2-aminoanthracene polyaromatic hydrocarbons (PAHs) into solution with resol and an F127 soft template.[256] Upon EISA, the PAHs assembled with the resol oligomers and initiated long-range graphitic layers due to their inherent planar structure. This method decreased the I_D/I_G of the neat MC from 1.48 to 0.7, 0.65, and 0.75 when using tetracycline, trihydroxyanthraquinone, and 2-aminoanthracene, respectively after carbonization at 900 °C. Therefore, the introduction of PAHs greatly enhanced the degree of graphitization of MC, while not significantly altering the pore characteristics of these carbons. Another method to increasing the degree of graphitization of MCs is to assemble highly graphitic particles within a carbon precursor during the soft-templating process. Fulvio et al. fabricated MCs through a soft templating approach with the presence of F127, resorcinol, and formaldehyde while also including conductive carbon black and carbon onions into the assembly process.[257] These conductive particles could replace up to 50 wt% of resol precursor, reducing the local energy requirement of graphitizing the carbon framework. It was found that the resorcinol/formaldehyde carbon precursors were physically adsorbed to the surface of the particles, allowing them to assemble within the hydrophilic domains of the template. The introduction of these carbon black additives did not greatly disrupt the pore structure but alter the pore size from 10 nm to 20 nm, depending on the loading level of the particle. These nanocomposites were then carbonized at 850 °C for 2 h and high degrees of graphitization were observed without requiring high carbonization temperatures.

6 | CONCLUSIONS AND OUTLOOK

Employing self-assembled polymers has now been widely used for fabricating MCs to potentially address a wide variety of different potential applications. This review focuses on discussing two primary approaches for producing MCs from nanostructured polymers, including through soft-templating method and direct pyrolysis strategy. The first one involves the use of surfactant molecules and/or BCPs for directing the nanostructure formation of carbon precursors, while the second approach can directly convert BCPs to MCs through rational design of BCP chemical compositions. Both methods require the crosslinking of selective components to enable their efficient conversion to carbon materials. Additionally, we discuss how to control the nanostructures of these MC systems by introducing the fundamental ordering mechanisms, methods for enabling their precise morphology and pore size control, as well as emerging approaches for producing directional pore channels within these MCs. These are all important aspects in the synthesis of polymer derived MCs as their performance and functionality are both directly related with the degree of ordering, alignment of their nanostructures, as well as pore textures. Furthermore, several common approaches to functionalize MCs are recognized and discussed for attaining enhanced performance, including activation for increasing surface areas, doping carbon framework for altering its physical properties, inclusion of nanoparticles, and increasing the graphitization degree of carbon walls for improving the electrical/thermal conductivity and mechanical integrity of MCs.

Looking forward, we want to provide a brief perspective on the research opportunities in the field of MCs derived from self-assembled polymers. Current works still focus on the synthesis of mesoporous carbons with tailored pore architectures such as a recent work from Lee et al. which developed highly aligned pore structures in lens-shaped particles.[258] While there are similar works focusing on developing MCs with desired performance, many current efforts regard providing new methodologies for the scaled production of MCs. It is important to note that compared to other carbon materials, such as activated carbons, graphene, graphene oxides, and carbon nanotubes, the commercialization opportunity of MCs is still underdeveloped, which may be associated with their high cost in the manufacturing process. For example, in soft-templating method at least three components (carbon precursor, template, and solvent) are required to be used, while measures also need to be taken for addressing solvent consumption and/or recovery, collectively leading to a total raw material cost that is likely at least one or two orders of magnitude higher than the activated carbons. Similarly, BCPs that can be directly employed as MC precursors often involve multiple steps of synthesis and purification, which sometimes could be challenging to scale up. As a result, despite the demonstrations of kilogram-scale synthesis and/or R2R based fabrication methods, MCs are still largely absent in most large-scale, practical systems. These fundamental limitations in MC production have led to multiple

works in solvent-free syntheses to provide a new "green" perspective, especially regarding the reduction of energy consumption and carbon footprint.[259-261] Additionally, several works explored the concept of using microwave synthesizer to prepare mesoporous carbons, which both crosslinking reaction and carbonization process can be significantly accelerated, reducing the reaction time from at least several hours to minutes.[233,262] However, microwave heating in most cases is driven by the high microwave cross-section of the substrate (instead of materials themselves), and therefore extending this approach to bulk MC manufacturing may be difficult.[263,264] We believe that fully unlocking the potential of MCs and enabling their efficient use in the practical applications necessitate some revolutionary advances in their manufacturing science.

ACKNOWLEDGMENTS

This work was partially supported by National Science Foundation Office of Integrative Activities #1757220. M.R. would like to acknowledge the support from NSF-NRT "Interface" program (DGE-1449999) through the University of Sothern Mississippi.

CONFLICT OF INTEREST

The authors declare no financial/commercial conflicts of interest.

ORCID

Zhe Qiang https://orcid.org/0000-0002-3539-9053

REFERENCES

[1] A. Stein, Z. Wang, M. A. Fierke, *Adv. Mater.* **2009**, *21*, 265.
[2] L. Chuenchom, R. Kraehnert, B. M. Smarsly, *Soft Matter* **2012**, *8*, 10801.
[3] H. W. Liang, X. Zhuang, S. Brüller, X. Feng, K. Müllen, *Nat. Commun.* **2014**, *5*, 4973.
[4] Q. Lai, Y. Zhao, Y. Liang, J. He, J. Chen, *Adv. Funct. Mater.* **2016**, *26*, 8334.
[5] H. Wang, Y. Shao, S. Mei, Y. Lu, M. Zhang, J. K. Sun, K. Matyjaszewski, M. Antonietti, J. Yuan, *Chem. Rev.* **2020**, *120*, 9363.
[6] B. Fang, J. H. Kim, M. S. Kim, J. S. Yu, *Acc. Chem. Res.* **2013**, *46*, 1397.
[7] R. W. Fu, Z. H. Li, Y. R. Liang, F. Li, F. Xu, D. C. Wu, *Xinxing Tan Cailiao/New Carbon Mater.* **2011**, *26*, 171.
[8] N. Mohamad Nor, L. C. Lau, K. T. Lee, A. R. Mohamed, *J. Environ. Chem. Eng.* **2013**, *1*, 658.
[9] S. Wong, N. Ngadi, I. M. Inuwa, O. Hassan, *J. Cleaner Prod.* **2018**, *175*, 361.
[10] Z. Heidarinejad, M. H. Dehghani, M. Heidari, G. Javedan, I. Ali, M. Sillanpää, *Environ. Chem. Lett.* **2020**, *18*, 393.
[11] P. González-García, *Renew. Sustain. Energy Rev.* **2018**, *82*, 1393.
[12] C. Liang, Z. Li, S. Dai, *Angew. Chem. Int. Ed.* **2008**, *47*, 3696.
[13] M. R. Benzigar, S. N. Talapaneni, S. Joseph, K. Ramadass, G. Singh, J. Scaranto, U. Ravon, K. Al-Bahily, A. Vinu, *Chem. Soc. Rev.* **2018**, *47*, 2680.
[14] T. Y. Ma, L. Liu, Z. Y. Yuan, *Chem. Soc. Rev.* **2013**, *42*, 3977.
[15] S. Tanaka, N. Nakatani, A. Doi, Y. Miyake, *Carbon* **2011**, *49*, 3184.
[16] C. H. Hou, X. Wang, C. Liang, S. Yiacoumi, C. Tsouris, S. Dai, *J. Phys. Chem. B* **2008**, *112*, 8563.
[17] L. Li, C. Song, H. Jiang, J. Qiu, T. Wang, *J. Membr. Sci.* **2014**, *450*, 469.
[18] A. Casanova, J. Iniesta, A. Gomis-Berenguer, *Analyst* **2022**, *147*, 767.
[19] J. Chrysostome Ndamanisha, L. Guo, *Anal. Chim. Acta* **2012**, *747*, 19.
[20] H. Li, D. Liu, X. Zhu, D. Qu, Z. Xie, J. Li, H. Tang, D. Zheng, D. Qu, *Nano Energy* **2020**, *73*, 104763.
[21] Y. Qu, M. Guo, X. Wang, C. Yuan, *J. Alloys Compd.* **2019**, *791*, 874.
[22] Z. W. Ding, D. L. Zhao, R. R. Yao, C. Li, X. W. Cheng, T. Hu, *Int. J. Hydrogen Energy* **2018**, *43*, 10502.
[23] Z. Qiang, X. Liu, F. Zou, K. A. Cavicchi, Y. Zhu, B. D. Vogt, *J. Phys. Chem. C* **2017**, *121*, 16702.
[24] A. Taguchi, F. Schüth, *Micropor. Mesopor. Mater.* **2005**, *77*, 1.
[25] R. Liu, X. Wang, X. Zhao, P. Feng, *Carbon* **2008**, *46*, 1664.
[26] Y. Wang, M. Liu, X. Zhao, D. Cao, T. Guo, B. Yang, *Carbon* **2018**, *135*, 238.
[27] H. J. Liu, W. J. Cui, L. H. Jin, C. X. Wang, Y. Y. Xia, *J. Mater. Chem.* **2009**, *19*, 3661.
[28] J. G. Wang, H. Liu, H. Sun, W. Hua, H. Wang, X. Liu, B. Wei, *Carbon* **2018**, *127*, 85.
[29] J. Wei, D. Zhou, Z. Sun, Y. Deng, Y. Xia, D. Zhao, *Adv. Funct. Mater.* **2013**, *23*, 2322.
[30] P. K. Tripathi, L. Gan, M. Liu, N. N. Rao, *J. Nanosci. Nanotechnol.* **2014**, *14*, 1823.
[31] M. Barczak, K. Michalak-Zwierz, K. Gdula, K. Tyszczuk-Rotko, R. Dobrowolski, A. Dąbrowski, *Micropor. Mesopor. Mater.* **2015**, *211*, 162.
[32] G. P. Hao, W. C. Li, S. Wang, S. Zhang, A. H. Lu, *Carbon* **2010**, *48*, 3330.
[33] Q. Sui, J. Huang, Y. S. Liu, X. F. Chang, G. B. Ji, S. Deng, *J. Environ. Sci.* **2011**, *23*, 177.
[34] R. Ryoo, S. H. Joo, M. Kruk, M. Jaroniec, *Adv. Mater.* **2001**, *13*, 677.
[35] Y. Wan, Y. Shi, D. Zhao, *Chem. Mater.* **2008**, *20*, 932.
[36] Y. Deng, J. Wei, Z. Sun, D. Zhao, *Chem. Soc. Rev.* **2013**, *42*, 4054.
[37] T. Liu, G. Liu, *J. Mater. Chem. A* **2019**, *7*, 23476.
[38] C. Li, Q. Li, Y. V. Kaneti, D. Hou, Y. Yamauchi, Y. Mai, *Chem. Soc. Rev.* **2020**, *49*, 4681.
[39] F. Bates, *Annu. Rev. Phys. Chem.* **1990**, *41*, 525.
[40] M. Robertson, Q. Zhou, C. Ye, Z. Qiang, *Macromol. Rapid Commun.* **2021**, *42*, 2100300.
[41] Y. Mai, A. Eisenberg, *Chem. Soc. Rev.* **2012**, *41*, 5969.
[42] C. Cummins, R. Lundy, J. J. Walsh, V. Ponsinet, G. Fleury, M. A. Morris, *Nano Today* **2020**, *35*, 100936.
[43] D. E. Jiang, A. C. T. Van Duin, W. A. Goddard, S. Dai, *J. Phys. Chem. A* **2009**, *113*, 6891.
[44] B. Saha, G. C. Schatz, *J. Phys. Chem. B* **2012**, *116*, 4684.
[45] Y. Meng, D. Gu, F. Zhang, Y. Shi, L. Cheng, D. Feng, Z. Wu, Z. Chen, Y. Wan, A. Stein, D. Zhao, *Chem. Mater.* **2006**, *18*, 4447.

[46] V. Chaudhary, S. Sharma, *J. Porous Mater.* **2017**, *24*, 741.
[47] V. L. Zholobenko, A. Y. Khodakov, M. Impéror-Clerc, D. Durand, I. Grillo, *Adv. Colloid Interface Sci.* **2008**, *142*, 67.
[48] S.-H. Wu, C.-Y. Mou, H.-P. Lin, *Chem. Soc. Rev.* **2013**, *42*, 3862.
[49] H. P. Lin, C. Y. Mou, *Acc. Chem. Res.* **2002**, *35*, 927.
[50] H. Chang, S. H. Joo, C. Pak, *J. Mater. Chem.* **2007**, *17*, 3078.
[51] S. Jain, F. S. Bates, *Science* **2003**, *300*, 460.
[52] C. M. Bates, F. S. Bates, *Macromolecules* **2017**, *50*, 3.
[53] M. Karayianni, S. Pispas, *J. Polym. Sci.* **2021**, *59*, 1874.
[54] C. T. Kresge, M. E. Leonowicz, W. J. Roth, J. C. Vartuli, J. S. Beck, *Nature* **1992**, *359*, 710.
[55] L. Song, D. Feng, N. J. Fredin, K. G. Yager, R. L. Jones, Q. Wu, D. Zhao, B. D. Vogt, *ACS Nano* **2010**, *4*, 189.
[56] Y. Wan, D. Zhao, *Chem. Rev.* **2007**, *107*, 2821.
[57] L. S. Romsted, Introduction to surfactant self-assembly. in *Supramolecular Chemistry*, Wiley Publications, NY, **2012**.
[58] S. Svenson, *Curr. Opin. Colloid Interface Sci.* **2004**, *9*, 201.
[59] D. P. Acharya, H. Kunieda, *Adv. Colloid Interface Sci.* **2006**, *123–126*, 401.
[60] R. Zana, Y. Talmon, *Nature* **1993**, *362*, 228.
[61] L. Leibler, H. Orland, J. C. Wheeler, *J. Chem. Phys.* **1983**, *79*, 3550.
[62] A. Chattopadhyay, E. London, *Anal. Biochem.* **1984**, *139*, 408.
[63] L. S. C. Wan, P. K. C. Poon, *J. Pharm. Sci.* **1969**, *58*, 1562.
[64] I. Astafieva, K. Khougaz, A. Eisenberg, *Macromolecules* **1995**, *28*, 7127.
[65] S. Chauhan, K. Sharma, *J. Chem. Thermodyn.* **2014**, *71*, 205.
[66] K. S. Birdi, S. Backlund, K. Sørensen, T. Krag, S. Dalsager, *J. Colloid Interface Sci.* **1978**, *66*, 118.
[67] S. Mehta, K. Bhasin, R. Chauhan, S. Dham, *Physicochem. Eng. Asp.* **2005**, *255*, 153.
[68] V. T. John, B. Simmons, G. L. Mcpherson, A. Bose, *Curr. Opin. Colloid Interface Sci.* **2002**, *7*, 288.
[69] I. Moriguchi, A. Ozono, K. Mikuriya, Y. Teraoka, S. Kagawa, M. Kodama, *Chem. Lett.* **1999**, *28*, 1171.
[70] Z. Li, W. Yan, S. Dai, *Carbon* **2004**, *42*, 767.
[71] M. Bruno, N. Cotella, M. Miras, T. Koch, S. Seidler, C. Barbero, *Colloids Surf. A Physicochem. Eng. Asp.* **2010**, *358*, 13.
[72] J. Chen, Y. Cheng, Q. Zhang, C. Fang, L. Wu, M. Bai, Y. Yao, *RSC Adv.* **2019**, *9*, 32258.
[73] M. W. Matsen, F. S. Bates, *Macromolecules* **1996**, *29*, 7641.
[74] C. J. Brinker, *MRS Bull.* **2004**, *29*, 631.
[75] M. Florent, C. Xue, D. Zhao, D. Goldfarb, *Chem. Mater.* **2012**, *24*, 383.
[76] F. Zhang, Y. Meng, D. Gu, Yan, Z. Chen, B. Tu, D. Zhao, *Chem. Mater.* **2006**, *18*, 5279.
[77] F. Zhang, Y. Meng, D. Gu, Yan, C. Yu, B. Tu, D. Zhao, *J. Am. Chem. Soc.* **2005**, *127*, 13508.
[78] Y. Lu, R. Ganguli, C. A. Drewien, M. T. Anderson, C. Jeffrey Brinker, W. Gong, Y. Guo, H. Soyez, B. Dunn, M. H. Huang, J. I. Zink, *Nature* **1997**, *389*, 364.
[79] S. A. Kim, K. J. Jeong, A. Yethiraj, M. K. Mahanthappa, *Proc. Natl. Acad. Sci. U. S. A.* **2017**, *114*, 4072.
[80] S. Chanpuriya, K. Kim, J. Zhang, S. Lee, A. Arora, K. D. Dorfman, K. T. Delaney, G. H. Fredrickson, F. S. Bates, *ACS Nano* **2016**, *10*, 4961.
[81] M. Huang, C. H. Hsu, J. Wang, S. Mei, X. Dong, Y. Li, M. Li, H. Liu, W. Zhang, T. Aida, W. B. Zhang, K. Yue, S. Z. D. Cheng, *Science* **2015**, *348*, 424.
[82] S. Lee, M. J. Bluemle, F. S. Bates, *Science* **2010**, *330*, 349.
[83] Y. Ding, K. R. Gadelrab, K. Mizrahi Rodriguez, H. Huang, C. A. Ross, A. Alexander-Katz, *Nat. Commun.* **2019**, *10*, 1.
[84] K. Yue, M. Huang, R. L. Marson, J. Hec, J. Huang, Z. Zhou, J. Wang, C. Liu, X. Yan, K. Wu, Z. Guo, H. Liu, W. Zhang, P. Ni, C. Wesdemiotis, W. B. Zhang, S. C. Glotzer, S. Z. D. Cheng, *Proc. Natl. Acad. Sci. U. S. A.* **2016**, *113*, 14195.
[85] K. Hayashida, T. Dotera, A. Takano, Y. Matsushita, *Phys. Rev. Lett.* **2007**, *98*, 195502.
[86] T. Z. Fermino, C. M. Awano, L. X. Moreno, D. R. Vollet, F. S. de Vicente, *Micropor. Mesopor. Mater.* **2018**, *267*, 242.
[87] Y. Fang, Y. Lv, R. Che, H. Wu, X. Zhang, D. Gu, G. Zheng, D. Zhao, *J. Am. Chem. Soc.* **2013**, *135*, 1524.
[88] Y. Zhai, Y. Dou, D. Zhao, P. F. Fulvio, R. T. Mayes, S. Dai, *Adv. Mater.* **2011**, *23*, 4828.
[89] Z. Qiang, B. Gurkan, J. Ma, X. Liu, Y. Guo, M. Cakmak, K. A. Cavicchi, B. D. Vogt, *Micropor. Mesopor. Mater.* **2016**, *227*, 57.
[90] X. Zhuang, Y. Wan, C. Feng, Y. Shen, D. Zhao, *Chem. Mater.* **2009**, *21*, 706.
[91] D. Feng, Y. Lv, Z. Wu, Y. Dou, L. Han, Z. Sun, Y. Xia, G. Zheng, D. Zhao, *J. Am. Chem. Soc.* **2011**, *133*, 51.
[92] J. Li, J. Qi, C. Liu, L. Zhou, H. Song, C. Yu, J. Shen, X. Sun, L. Wang, *J. Mater. Chem. A* **2014**, *2*, 4144.
[93] E. Ramasamy, J. Chun, J. Lee, *Carbon* **2010**, *48*, 4563.
[94] L. L. Shao, M. Chen, Z. Y. Yuan, *J. Power Sources* **2014**, *272*, 1091.
[95] Y. Song, L. Li, Y. Wang, C. Wang, Z. Guo, Y. Xia, *ChemPhysChem* **2014**, *15*, 2084.
[96] Q. Li, R. Jiang, Y. Dou, Z. Wu, T. Huang, D. Feng, J. Yang, A. Yu, D. Zhao, *Carbon* **2011**, *49*, 1248.
[97] H. Javed, S. Pani, J. Antony, M. Sakthivel, J.-F. Drillet, *Soft Matter* **2021**, *17*, 7743.
[98] L. Hu, C. Wang, L. Ye, Y. Wu, B. Yue, X. Chen, H. He, *Appl. Catal. A Gen.* **2015**, *504*, 440.
[99] X. Wan, Y. Li, H. Xiao, Y. Pan, J. Liu, *RSC Adv.* **2020**, *10*, 2932.
[100] R. Liu, Y. Shi, Y. Wan, Y. Meng, F. Zhang, D. Gu, Z. Chen, B. Tu, D. Zhao, *J. Am. Chem. Soc.* **2006**, *128*, 11652.
[101] J. Wang, C. Xue, Y. Lv, F. Zhang, B. Tu, D. Zhao, *Carbon* **2011**, *49*, 4580.
[102] Z. Qiang, Y. Guo, H. Liu, S. Z. D. Cheng, M. Cakmak, K. A. Cavicchi, B. D. Vogt, *ACS Appl. Mater. Interfaces* **2015**, *7*, 4306.
[103] J. Zhang, Y. Deng, J. Wei, Z. Sun, D. Gu, H. Bongard, C. Liu, H. Wu, B. Tu, F. Sch, D. Zhao, *Chem. Mater.* **2009**, *21*, 3996.
[104] J. Lee, J. Shim, J. Lee, Y. Ye, J. Hwang, S. K. Kim, T. H. Lim, U. Wiesner, *ACS Nano* **2012**, *6*, 6870.
[105] Y. Deng, Y. Cai, Z. Sun, D. Gu, J. Wei, W. Li, X. Guo, J. Yang, D. Zhao, *Adv. Funct. Mater.* **2010**, *20*, 3658.
[106] Z. Wang, Y. Zhu, W. Luo, Y. Ren, X. Cheng, P. Xu, X. Li, Y. Deng, D. Zhao, *Chem. Mater.* **2016**, *28*, 7773.
[107] Y. Li, J. Wei, W. Luo, C. Wang, W. Li, S. Feng, Q. Yue, M. Wang, A. A. Elzatahry, Y. Deng, D. Zhao, *Chem. Mater.* **2014**, *26*, 2438.
[108] K. Matyjaszewski, *Macromolecules* **2012**, *45*, 4015.
[109] S. Perrier, *Macromolecules* **2017**, *50*, 7433.
[110] Y. Deng, T. Yu, Y. Wan, Y. Shi, Y. Meng, D. Gu, L. Zhang, Y. Huang, C. Liu, X. Wu, D. Zhao, *J. Am. Chem. Soc.* **2007**, *129*, 1690.

[111] Y. Deng, C. Liu, D. Gu, T. Yu, B. Tu, D. Zhao, *J. Mater. Chem.* **2008**, *18*, 91.
[112] J. G. Li, Y. F. Ho, M. M. M. Ahmed, H. C. Liang, S. W. Kuo, *Chem. Eur. J.* **2019**, *25*, 10456.
[113] W. C. Chu, B. P. Bastakoti, Y. V. Kaneti, J. G. Li, H. R. Alamri, Z. A. Alothman, Y. Yamauchi, S. W. Kuo, *Chem. Eur. J.* **2017**, *23*, 13734.
[114] J. G. Li, C. Y. Chung, S. W. Kuo, *J. Mater. Chem.* **2012**, *22*, 18583.
[115] Y. R. Liu, *Micropor. Mesopor. Mater.* **2009**, *124*, 190.
[116] J. G. Li, W. C. Chu, U. S. Jeng, S. W. Kuo, *Macromol. Chem. Phys.* **2013**, *214*, 2115.
[117] Q. Zhang, F. Matsuoka, H. S. Suh, P. A. Beaucage, S. Xiong, D.-M. Smilgies, Kwan, W. Tan, Jö, G. Werner, P. F. Nealey, U. B. Wiesner, *ACS Nano* **2018**, *12*, 19.
[118] G. Deng, Z. Qiang, W. Lecorchick, K. A. Cavicchi, B. D. Vogt, *Langmuir* **2014**, *30*, 2530.
[119] P. Li, Y. Song, Z. Tang, G. Yang, J. Yang, *J. Colloid Interface Sci.* **2014**, *413*, 154.
[120] Y. Liu, *J. Porous Mater.* **2011**, *18*, 597.
[121] C. Liang, K. Hong, G. A. Guiochon, J. W. Mays, S. Dai, *Angew. Chem. Int. Ed.* **2004**, *43*, 5785.
[122] H. Kosonen, S. Valkama, A. Nykänen, M. Toivanen, G. ten Brinke, J. Ruokolainen, O. Ikkala, *Adv. Mater.* **2006**, *18*, 201.
[123] Z. Qiang, J. Xue, K. A. Cavicchi, B. D. Vogt, *Langmuir* **2013**, *29*, 3428.
[124] Z. Qiang, J. Xue, G. E. Stein, K. A. Cavicchi, B. D. Vogt, *Langmuir* **2013**, *29*, 8703.
[125] A. Gregory, M. H. Stenzel, *Prog. Polym. Sci.* **2012**, *37*, 38.
[126] Y. Gao, D. Zhou, J. Lyu, A. Sigen, Q. Xu, B. Newland, K. Matyjaszewski, H. Tai, W. Wang, *Nat. Rev. Chem.* **2020**, *4*, 194.
[127] R. Verduzco, X. Li, S. L. Pesek, G. E. Stein, *Chem. Soc. Rev.* **2015**, *44*, 2405.
[128] G. Xie, M. R. Martinez, M. Olszewski, S. S. Sheiko, K. Matyjaszewski, *Biomacromolecules* **2019**, *20*, 27.
[129] R. Fenyves, M. Schmutz, I. J. Horner, F. V. Bright, J. Rzayev, *J. Am. Chem. Soc.* **2014**, *136*, 7762.
[130] Y. Gai, D.-P. Song, B. M. Yavitt, J. J. Watkins, *Macromolecules* **2017**, *50*, 1503.
[131] Z. Li, M. Tang, S. Liang, M. Zhang, G. M. Biesold, Y. He, S. M. Hao, W. Choi, Y. Liu, J. Peng, Z. Lin, *Prog. Polym. Sci.* **2021**, *116*, 101387.
[132] A. L. Liberman-Martin, C. K. Chu, R. H. Grubbs, *Macromol. Rapid Commun.* **2017**, *38*, 1.
[133] T. Guo, Y. Wang, Y. Qiao, X. Yuan, Y. Zhao, L. Ren, *Polymer* **2020**, *194*, 122389.
[134] D. F. Sunday, M. Dolejsi, A. B. Chang, L. J. Richter, R. Li, R. J. Kline, P. F. Nealey, R. H. Grubbs, *ACS Nano* **2020**, *14*, 17476.
[135] P. T. III, J. W. Thackeray, G. Sun, S. Cho, C. Clark, S. V. Verkhoturov, M. J. Eller, A. Li, A. Pavia-Sanders, E. A. Schweikert, K. L. Wooley, *J. Micro/Nanolithogr. MEMS MOEMS* **2013**, *12*, 043006.
[136] E. J. Kim, J. J. Shin, T. Do, G. S. Lee, J. Park, V. Thapar, J. Choi, J. Bang, G.-R. Yi, S.-M. Hur, J. G. Kim, B. J. Kim, *ACS Nano* **2021**, *15*, 17.
[137] K. Zhao, Z. Gao, D. Song, P. Zhang, J. Cui, *Polym. Chem.* **2022**, *13*, 373.
[138] K. Miki, K. Oride, A. Kimura, Y. Kuramochi, H. Matsuoka, H. Harada, M. Hiraoka, K. Ohe, *Small* **2011**, *7*, 3536.
[139] K. Miki, A. Kimura, K. Oride, Y. Kuramochi, H. Matsuoka, H. Harada, M. Hiraoka, K. Ohe, *Angew. Chem. Int. Ed.* **2011**, *50*, 6567.
[140] H. F. Fei, W. Li, A. Bhardwaj, S. Nuguri, A. Ribbe, J. J. Watkins, *J. Am. Chem. Soc.* **2019**, *141*, 17006.
[141] H.-F. Fei, W. Li, S. Nuguri, H.-J. Yu, B. M. Yavitt, W. Fan, J. J. Watkins, *Chem. Mater.* **2020**, *32*, 6055.
[142] A. Bhardwaj, J. N. Pagaduan, Y.-G. Yu, V. J. Einck, S. Nuguri, R. Katsumata, J. J. Watkins, *ACS Appl. Mater. Interfaces* **2021**, *13*, 61027.
[143] H. F. Fei, Y. Long, H. J. Yu, B. M. Yavitt, W. Fan, A. Ribbe, J. J. Watkins, *ACS Appl. Mater. Interfaces* **2020**, *12*, 57322.
[144] M. Nemanashi, J. H. Noh, R. Meijboom, *J. Mater. Sci.* **2018**, *53*, 12663.
[145] M. C. Rogers, B. Adisa, D. A. Bruce, *Catal. Lett.* **2004**, *98*, 29.
[146] A. Gupta, I. R. Harrison, *Carbon N. Y.* **1997**, *35*, 809.
[147] Z. Wangxi, L. Jie, W. Gang, *Carbon N. Y.* **2003**, *41*, 2805.
[148] X. Liu, Y. Makita, Y. L. Hong, Y. Nishiyama, T. Miyoshi, *Macromolecules* **2017**, *50*, 244.
[149] X. Liu, W. Chen, Y. L. Hong, S. Yuan, S. Kuroki, T. Miyoshi, *Macromolecules* **2015**, *48*, 5300.
[150] L. Li, K. Raghupathi, C. Song, P. Prasad, S. Thayumanavan, *Chem. Commun.* **2014**, *50*, 13417.
[151] M. Kopeć, M. Lamson, R. Yuan, C. Tang, M. Kruk, M. Zhong, K. Matyjaszewski, T. Kowalewski, *Prog. Polym. Sci.* **2019**, *92*, 89.
[152] R. Yi, Y. Song, C. Wu, G. Wei, R. Yuan, Y. Chen, G. Ye, T. Kowalewski, K. Matyjaszewski, *ACS Appl. Bio Mater.* **2020**, *3*, 1036.
[153] C. K. Kim, H. Zhou, T. Kowalewski, K. Matyjaszewski, H. K. Kim, *ACS Appl. Mater. Interfaces* **2019**, *11*, 2093.
[154] C. Tang, T. Kowaleweki, K. Matyjaszewski, *Macromolecules* **2003**, *36*, 1465.
[155] Y. Wang, L. B. Kong, X. M. Li, F. Ran, Y. C. Luo, L. Kang, *Xinxing Tan Cailiao/New Carbon Mater.* **2015**, *30*, 302.
[156] F. Ran, K. Shen, Y. Tan, B. Peng, S. Chen, W. Zhang, X. Niu, L. Kong, L. Kang, *J. Membr. Sci.* **2016**, *514*, 366.
[157] C. T. Nguyen, D. P. Kim, *J. Mater. Chem.* **2011**, *21*, 14226.
[158] Z. Zhou, G. Liu, *Small* **2017**, *13*, 1603107.
[159] M. Stefik, J. Lee, U. Wiesner, *Chem. Commun.* **2009**, 2532.
[160] T. Kowalewski, N. V. Tsarevsky, K. Matyjaszewski, *J. Am. Chem. Soc.* **2002**, *124*, 10632.
[161] A. Palanisamy, N. V. Salim, B. L. Fox, P. Jyotishkumar, T. Pradeep, N. Hameed, *RSC Adv.* **2016**, *6*, 55792.
[162] R. Yuan, M. Kopeć, G. Xie, E. Gottlieb, J. W. Mohin, Z. Wang, M. Lamson, T. Kowalewski, K. Matyjaszewski, *Polymer* **2017**, *126*, 352.
[163] D. Wu, Z. Li, M. Zhong, T. Kowalewski, K. Matyjaszewski, *Angew. Chem. Int. Ed.* **2014**, *53*, 3957.
[164] Z. Zhou, T. Liu, A. U. Khan, G. Liu, *Sci. Adv.* **2019**, *5*, eaau6852.
[165] T. Liu, J. Serrano, J. Elliott, X. Yang, W. Cathcart, Z. Wang, Z. He, G. Liu, *Sci. Adv.* **2020**, *6*, aaz0906.
[166] Z. Zhou, T. Liu, A. U. Khan, G. Liu, *Mol. Syst. Des. Eng.* **2020**, *5*, 153.
[167] T. Liu, Z. Zhou, Y. Guo, D. Guo, G. Liu, *Nat. Commun.* **2019**, *10*, 675.
[168] J. M. Serrano, A. U. Khan, T. Liu, Z. Xu, A. R. Esker, G. Liu, *Adv. Mater. Interfaces* **2020**, *7*, 2000507.

[169] W. Zhao, Z. Xu, J. Elliott, C. S. Barrera, Z. L. Croft, H. Zhao, J. Tardiff, G. Liu, *ACS Appl. Polym. Mater.* **2021**, *3*, 6019.
[170] J. Yang, Y. Bao, P. Pan, *Mater. Sci.* **2014**, *49*, 1090.
[171] C. Zou, D. Wu, M. Li, Q. Zeng, F. Xu, Z. Huang, R. Fu, *J. Mater. Chem.* **2010**, *20*, 731.
[172] X. Zhang, S. Shen, L. Fan, *J. Mater. Sci.* **2007**, *42*, 7621.
[173] Z. Li, D. Wu, X. Huang, J. Ma, H. Liu, Y. Liang, R. Fu, K. Matyjaszewski, *Energy Environ. Sci.* **2014**, *7*, 3006.
[174] Y. S. Sun, W. H. Huang, J. Y. Liou, Y. H. Lu, K. C. Shih, C. F. Lin, S. L. Cheng, *RSC Adv.* **2015**, *5*, 105774.
[175] M. Inagaki, N. Ohta, Y. Hishiyama, *Carbon* **2013**, *61*, 1.
[176] H. Hatori, T. Kobayashi, Y. Hanzawa, Y. Yamada, Y. Iimura, T. Kimura, M. Shiraishi, *J. Appl. Polym. Sci.* **2001**, *79*, 836.
[177] F. Xu, D. Wu, R. Fu, B. Wei, *Mater. Today* **2017**, *20*, 629.
[178] T. P. Fellinger, A. Thomas, J. Yuan, M. Antonietti, *Adv. Mater.* **2013**, *25*, 5838.
[179] V. Malgras, J. Tang, J. Wang, J. Kim, N. L. Torad, S. Dutta, K. Ariga, M. S. A. Hossain, Y. Yamauchi, K. C. W. Wu, *J. Nanosci. Nanotechnol.* **2019**, *19*, 3673.
[180] G. Sun, J. Wang, X. Liu, D. Long, W. Qiao, L. Ling, *J. Phys. Chem. C* **2010**, *114*, 18745.
[181] M. Karthik, E. Redondo, E. Goikolea, V. Roddatis, S. Doppiu, R. Mysyk, *J. Phys. Chem. C* **2014**, *118*, 27715.
[182] D. D. Asouhidou, K. S. Triantafyllidis, N. K. Lazaridis, K. A. Matis, S. S. Kim, T. J. Pinnavaia, *Micropor. Mesopor. Mater.* **2009**, *117*, 257.
[183] M. Inagaki, M. Toyoda, Y. Soneda, S. Tsujimura, T. Morishita, *Carbon* **2016**, *107*, 448.
[184] H. Cui, Z. Chen, S. Zhong, K. L. Wooley, D. J. Pochan, *Science* **2007**, *317*, 647.
[185] J. C. Brendel, F. H. Schacher, *Chem. Asian J.* **2018**, *13*, 230.
[186] G. Wang, Y. Liu, Y. Liu, N. Xia, W. Zhou, Q. Gao, S. Liu, *Colloids Surf. A Physicochem. Eng. Asp.* **2017**, *529*, 808.
[187] M. Li, S. Mann, *Angew. Chem. Int. Ed.* **2008**, *47*, 9476.
[188] W.-C. Chu, S.-F. Chiang, J.-G. Li, S.-W. Kuo, *Materials* **2013**, *6*, 5077.
[189] J. Schuster, R. Köhn, M. Döblinger, A. Keilbach, H. Amenitsch, T. Bein, *J. Am. Chem. Soc.* **2012**, *134*, 11136.
[190] Y. Zhang, Z. Qiang, B. D. Vogt, *RSC Adv.* **2014**, *4*, 44858.
[191] A. Labiano, M. Dai, W. S. Young, G. E. Stein, K. A. Cavicchi, T. H. Epps, B. D. Vogt, *J. Phys. Chem. C* **2012**, *116*, 6038.
[192] J. N. L. Albert, T. H. Epps, *Mater. Today* **2010**, *13*, 24.
[193] M. J. Fasolka, A. M. Mayes, *Annu. Rev. Mater. Sci.* **2001**, *31*, 323.
[194] G. Deng, Y. Zhang, C. Ye, Z. Qiang, G. E. Stein, K. A. Cavicchi, B. D. Vogt, *Chem. Commun.* **2014**, *50*, 12684.
[195] Y. Meng, D. Gu, F. Zhang, Y. Shi, H. Yang, Z. Li, C. Yu, B. Tu, D. Zhao, *Angew. Chem. Int. Ed.* **2005**, *44*, 7053.
[196] J. Wei, Z. JSun, W. Luo, Y. Li, A. A. Elzatahry, A. M. Al-Enizi, Y. Deng, D. Zhao, *J. Am. Chem. Soc.* **2017**, *139*, 1706.
[197] M. Kruk, *Acc. Chem. Res.* **2012**, *45*, 1678.
[198] Y. Deng, J. Liu, C. Liu, D. Gu, Z. Sun, J. Wei, J. Zhang, L. Zhang, B. Tu, D. Zhao, *Chem. Mater.* **2008**, *20*, 7281.
[199] M. Trivedi, F. Peng, X. Xia, P. I. Sepulveda-Medina, B. D. Vogt, *Langmuir,* **2019**, *35*, 14049.
[200] J. P. Hanrahan, M. P. Copley, K.M. Ryan, T. R. Spalding, M. A. Morris, J. D. Holmes, *Chem. Mater.* **2004**, *16*, 424.
[201] X. Gu, I. Gunkel, A. Hexemer, W. Gu, T. P Russell, *Adv. Mater,* **2014**, *26*, 273.
[202] R. Wang, K. Lan, R. Lin, X. Jing, C. Te Hung, X. Zhang, L. Liu, Y. Yang, G. Chen, X. Liu, C. Fan, A. M. El-Toni, A. Khan, Y. Tang, D. Zhao, *ACS Nano* **2021**, *15*, 7713.
[203] Z. Qiang, Y. Zhang, Y. Wang,S. M. Bhaway, K. A. Cavicchi, B. D. Vogt, *Carbon* **2015**, *82*, 51.
[204] Z. Qiang, Y. Zhang, J. A. Groff, K. A. Cavicchi, B. D. Vogt, *Soft Matter* **2014**, *10*, 1109.
[205] J. Xue, G. Singh, Z. Qiang, A. Karim, B. D. Vogt, *Nanoscale* **2013**, *5*, 7928.
[206] J. Xue, G. Singh, Z. Qiang, K. G. Yager, A. Karim, B. D. Vogt, *Nanoscale* **2013**, *5*, 12440.
[207] K. G. Yager, N. J. Fredin, X. Zhang, B. C. Berry, A. Karim, R. L. Jones, *Soft Matter* **2009**, *6*, 92.
[208] G. Singh, K. G. Yager, B. Berry, H. C. Kim, A. Karim, *ACS Nano* **2012**, *6*, 10335.
[209] G. Singh, K. G. Yager, D. M. Smilgies, M. M. Kulkarni, D. G. Bucknall, A. Karim, *Macromolecules* **2012**, *45*, 7107.
[210] B. C. Berry, A. W. Bosse, J. F. Douglas, R. L. Jones, A. Karim, *Nano Lett.* **2007**, *7*, 2789.
[211] J. Gu, R. Zhang, L. Zhang, J. Lin, *Macromolecules* **2020**, *53*, 2111.
[212] C. Tang, A. Tracz, M. Kruk, R. Zhang, D. M. Smilgies, K. Matyjaszewski, T. Kowalewski, *J. Am. Chem. Soc.* **2005**, *127*, 6918.
[213] G. Singh, S. Batra, R. Zhang, H. Yuan, K. G. Yager, M. Cakmak, B. Berry, A. Karim, *ACS Nano* **2013**, *7*, 5291.
[214] Y. Wu, X. Lu, Q. Lu, *Micropor. Mesopor. Mater.* **2015**, *211*, 152.
[215] S. K. Singh, K. Takeyasu, J. Nakamura, *Adv. Mater.* **2019**, *31*, 1804297.
[216] Y. Deng, Y. Xie, K. Zou, X. Ji, *J. Mater. Chem. A* **2016**, *4*, 1144.
[217] V. Perazzolo, C. Durante, A. Gennaro, *J. Electroanal. Chem.* **2016**, *782*, 264.
[218] W. Kiciński, M. Szala, M. Bystrzejewski, *Carbon* **2014**, *68*, 1.
[219] P. Lawtae, C. Tangsathitkulchai, *Molecules* **2021**, *26*, 2758.
[220] Z. Bao, M. K. Song, S. C. Davis, Y. Cai, M. Liu, K. H. Sandhage, *Energy Environ. Sci.* **2011**, *4*, 3980.
[221] M. Cox, R. Mokaya, *Sustain. Energy Fuels* **2017**, *1*, 1414.
[222] M. Sevilla, R. Mokaya, A. B. Fuertes, *Energy Environ. Sci.* **2011**, *4*, 2930.
[223] M. Choi, R. Ryoo, *J. Mater. Chem.* **2007**, *17*, 4204.
[224] Y. Lv, F. Zhang, Y. Dou, Y. Zhai, J. Wang, H. Liu, Y. Xia, B. Tu, D. Zhao, *J. Mater. Chem.* **2012**, *22*, 93.
[225] Z. He, G. Zhang, Y. Chen, Y. Xie, T. Zhu, H. Guo, Y. Chen, *J. Mater. Sci.* **2017**, *52*, 2422.
[226] K. Xia, Q. Gao, C. Wu, S. Song, M. Ruan, *Carbon* **2007**, *45*, 1989.
[227] J. Ludwinowicz, M. Jaroniec, *Carbon* **2015**, *94*, 673.
[228] X. Xu, C. Shi, R. Chen, T. Chen, *RSC Adv.* **2017**, *7*, 22263.
[229] B. Bayatsarmadi, Y. Zheng, M. Jaroniec, S. Z. Qiao, *Chem. Asian J.* **2015**, *10*, 1546.
[230] W. Song, J. Kan, H. Wang, X. Zhao, Y. Zheng, H. Zhang, L. Tao, M. Huang, W. Liu, J. Shi, *ACS Appl. Nano Mater.* **2019**, *2*, 5643.
[231] D. Kim, G. Kim, S. Oh, J. Park, S. Lee, S. Yoon, J. Lee, W. Lee, T. Y. Jeon, E. Cho, K. Sohn, D. K. Yang, J. Kim, *ACS Sustain. Chem. Eng.* **2020**, *8*, 8537.
[232] F. Wang, J. Xu, X. Shao, X. Su, Y. Huang, T. Zhang, *ChemSusChem* **2016**, *9*, 246.

[233] U. Jeong, H. J. Kim, S. Ramesh, N. A. Dogan, S. Wongwilawan, S. Kang, J. Park, E. S. Cho, C. T. Yavuz, *Angew. Chem. Int. Ed.* **2021**, *60*, 22478.
[234] M. Naushad, T. Ahamad, B. M. Al-Maswari, A. Abdullah Alqadami, S. M. Alshehri, *Chem. Eng. J.* **2017**, *330*, 1351.
[235] M. X. Liu, X. X. Deng, D. Z. Zhu, H. Duan, W. Xiong, Z. J. Xu, L. H. Gan, *Chin. Chem. Lett.* **2016**, *27*, 795.
[236] J. Yu, M. Guo, F. Muhammad, A. Wang, F. Zhang, Q. Li, G. Zhu, *Carbon* **2014**, *69*, 502.
[237] S. Shrestha, N. Morse, W. E. Mustain, *RSC Adv.* **2014**, *4*, 47039.
[238] J. Du, Y. Yu, L. Liu, H. Lv, A. Chen, S. Hou, *ACS Appl. Energy Mater.* **2019**, *2*, 4402.
[239] M. Duan, F. Zhu, G. Zhao, J. Hu, H. Zhang, G. Ren, Y. Meng, Z. Fan, *Micropor. Mesopor. Mater.* **2020**, *306*, 110433.
[240] T. Jiang, Y. Wang, K. Wang, Y. Liang, D. Wu, P. Tsiakaras, S. Song, *Appl. Catal. B Environ.* **2016**, *189*, 1.
[241] X. Wang, C. G. Liu, D. Neff, P. F. Fulvio, R. T. Mayes, A. Zhamu, Q. Fang, G. Chen, H. M. Meyer, B. Z. Jang, S. Dai, *J. Mater. Chem. A* **2013**, *1*, 7920.
[242] R. Xing, Y. Liu, Y. Wang, L. Chen, H. Wu, Y. Jiang, M. He, P. Wu, *Micropor. Mesopor. Mater.* **2007**, *105*, 41.
[243] H. Xue, T. Wang, J. Zhao, H. Gong, J. Tang, H. Guo, X. Fan, J. He, *Carbon* **2016**, *104*, 10.
[244] Z. Qiang, Y. Xia, X. Xia, B. D. Vogt, *Chem. Mater.* **2017**, *29*, 10178.
[245] Z. Qiang, Y. M. Chen, Y. Xia, W. Liang, Y. Zhu, B. D. Vogt, *Nano Energy* **2017**, *32*, 59.
[246] V. Jose, A. Jayakumar, J. M. Lee, *ChemElectroChem* **2019**, *6*, 1485.
[247] H. Jiang, J. Ma, C. Li, *Adv. Mater.* **2012**, *24*, 4197.
[248] T. Yamamoto, S. I. Kim, J. Chaichanawong, E. Apiluck, T. Ohmori, *Appl. Catal. B Environ.* **2009**, *88*, 455.
[249] K. W. Staggs, Z. Qiang, K. Madathil, C. Gregson, Y. Xia, B. Vogt, D. R. Nielsen, *ACS Sustain. Chem. Eng.* **2017**, *5*, 885.
[250] J. Li, J. Gu, H. Li, Y. Liang, Y. Hao, X. Sun, L. Wang, *Micropor. Mesopor. Mater.* **2010**, *128*, 144.
[251] Y. Chen, C. Ma, Y. Wu, C. Ke, X. Liu, J. Wang, W. Qiao, L. Ling, *Micropor. Mesopor. Mater.* **2022**, *333*, 111712.
[252] A. García, A. Nieto, M. Vila, M. Vallet-Regí, *Carbon* **2013**, *51*, 410.
[253] Z. Qiang, Y. M. Chen, B. Gurkan, Y. Guo, M. Cakmak, K. A. Cavicchi, Y. Zhu, B. D. Vogt, *Carbon* **2017**, *116*, 286.
[254] D. Li, H. Wang, X. Wang, *J. Mater. Sci.* **2007**, *42*, 4642.
[255] J. Tang, T. Wang, X. Sun, Y. Guo, H. Xue, H. Guo, M. Liu, X. Zhang, J. He, *Micropor. Mesopor. Mater.* **2013**, *177*, 105.
[256] A. Beitollahi, M. A. S. Sheikhaleslami, *Carbon* **2016**, *107*, 440.
[257] P. F. Fulvio, R. T. Mayes, X. Wang, S. M. Mahurin, J. C. Bauer, V. Presser, J. Mcdonough, Y. Gogotsi, S. Dai, *Adv. Funct. Mater.* **2011**, *21*, 2208.
[258] Y. J. Lee, H. E. Kim, H. Oh, H. Yun, J. Lee, S. Shin, H. Lee, B. J. Kim, *ACS Nano* **2022**, *16*, 2988.
[259] X. Kan, F. Song, F. Li, S. Xiao, F. Liu, L. Jiang, *J. Mater. Chem. A* **2022**, Advance Article. https://doi.org/10.1039/D2TA00408A.
[260] X. Liu, Y. Zhou, C. L. Wang, Y. Liu, D. J. Tao, *Chem. Eng. J.* **2022**, *427*, 130878.
[261] P. Zhang, L. Wang, S. Yang, J. A. Schott, X. Liu, S. M. Mahurin, C. Huang, Y. Zhang, P. F. Fulvio, M. F. Chisholm, S. Dai, *Nat. Commun.* **2017**, *8*, 1.
[262] X. Xia, C. F. Cheng, Y. Zhu, B. D. Vogt, *Micropor. Mesopor. Mater.* **2021**, *310*, 110639.
[263] Y. Xia, Z. Qiang, B. Lee, M. L. Becker, B. D. Vogt, *CrystEngComm* **2017**, *19*, 4294.
[264] Z. Qiang, C. Ye, K. Lin, M. L. Becker, K. A. Cavicchi, B. D. Vogt, *J. Polym. Sci. Part B: Polym. Phys.* **2016**, *54*, 1499.

AUTHOR BIOGRAPHIES

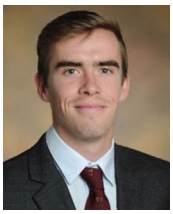

Mark Robertson completed his BS in Chemical Engineering at the University of Mississippi in 2019. He joined the Polymer Science and Engineering program at the University of Southern Mississippi in 2019 and is currently a PhD student in the Qiang research group. His research focuses on block copolymer self-assembly, and a breadth of block copolymer derived functional materials.

Moustafa M. Zagho received his MS in Chemistry in 2015 from Alexandria University. He worked as a research assistant at Qatar University (2013–2017). Currently, he is a PhD student in Polymer Science and Engineering at the University of Southern Mississippi, designing water filtration membranes, and thermally conductive polymer composites using bioinspired materials.

Sergei Nazarenko received his BS degree in Molecular and Chemical Physics from Moscow Institute of Physics and Technology, and PhD in Physics and Mathematics from the Semenov Institute of Chemical Physics of Russian Academy of Sciences. He carried out postdoctoral work in the Department of Macromolecular Science and Engineering at Case Western Reserve University before joining the faculty in the same department. In 2004, Dr. Nazarenko moved to the University of Southern Mississippi where he currently is a Full Professor of Polymer Science and Engineering. Dr. Nazarenko's research interests include transport phenomena in polymers, gas permeation, probing and modeling of free volume, and development of advanced polymeric materials for energy, sustainability, and safety.

Zhe Qiang is an Assistant Professor of Polymer Science and Engineering at the University of Southern Mississippi. He received his MS and PhD degrees in Polymer Engineering from the University of Akron, and was a postdoc fellow at Northwestern University. His current research interests include self-assembly and interfacial phenomenon in soft matter and composites, including in-situ characterization of polymer chain conformations and nanostructures and manufacturing of functional porous materials for energy and environmental applications.

How to cite this article: M. Robertson, M. M. Zagho, S. Nazarenko, Z. Qiang, *J. Polym. Sci.* **2022**, *60*(14), 2015. https://doi.org/10.1002/pol.20220122